

# SMARCPAD: A Smart Seat Pad for Cycling Fitness Tracking Leveraging Low-cost Conductive Fabric Sensors

YI WU\*, University of Tennessee, Knoxville, USA

LUIS ALONSO GONZÁLEZ VILLALOBOS\*, University of Tennessee, Knoxville, USA

ZHENNING YANG, University of Tennessee, Knoxville, USA

GREGORY THOMAS CROISDALE, University of Tennessee, Knoxville, USA

ÇAĞDAŞ KARATAŞ, Microsoft, USA

JIAN LIU, University of Tennessee, Knoxville, USA

Cycling is an efficient and effective way to improve one's overall fitness level, such as cardiovascular fitness, stamina, lower body strength, and body fat percentage. To improve fitness performance, real-time cycling fitness tracking can not only allow cyclists to better control their energy outputs but also help push workout intensity and keep users accountable for their fitness progress. However, existing bike sensors (e.g., the ones mounted to bike's wheel hub or crank arm) are only limited to measuring cycling cadence and speed. Although several recent studies relying on on-body sensors or cameras can provide more fine-grained information (e.g., riding position and knee joint angle), they would either require inconvenient setups or raise serious privacy concerns. To circumvent these limitations, in this paper, we propose SMARCPAD, an innovative smart seat pad that can continuously and unobtrusively track five cycling-specific metrics, including cadence, per-leg stability, leg strength balance, riding position, and knee joint angle of the cyclist. Specifically, we embed conductive fabric sensors in the seat pad to sense the pressure applied to the bike's seat exerted by the cyclist's gluteal muscles. A series of signal processing algorithms are developed to estimate the pedaling period from the sensed pressure signal and further derive the cycling cadence, per-leg stability, and leg strength balance. Additionally, we leverage a deep learning model to detect the cyclist's riding position and reconstruct the cyclist's knee joint angles via linear regression. The sensors and the system prototype are manufactured from scratch leveraging off-the-shelf materials, and the total cost is less than \$50. Extensive experiments involving 15 participants demonstrate that SMARCPAD can accurately estimate the cycling cadence with an average error of 1.13 rounds per minute, quantify the cycling stability for each leg, detect cycling imbalance, distinguish five riding positions with an accuracy of 96.60%, and continuously track the knee joint angle with an average mean error as low as 9.58 degrees.

CCS Concepts: • Human-centered computing → Ubiquitous and mobile computing.

Additional Key Words and Phrases: mobile computing, fabric sensing, cycling fitness tracking

## ACM Reference Format:

Yi Wu, Luis Alonso González Villalobos, Zhenning Yang, Gregory Thomas Croisdale, Çağdaş KARATAŞ, and Jian Liu. 2023. SMARCPAD: A Smart Seat Pad for Cycling Fitness Tracking Leveraging Low-cost Conductive Fabric Sensors. *Proc. ACM Interact. Mob. Wearable Ubiquitous Technol.* 7, 3, Article 135 (September 2023), 26 pages. <https://doi.org/10.1145/3610927>

\*Both authors contributed equally to this research.

---

Authors' addresses: Yi Wu, University of Tennessee, Knoxville, Knoxville, USA, ywu83@vols.utk.edu; Luis Alonso González Villalobos, lgonzal6@vols.utk.edu, University of Tennessee, Knoxville, Knoxville, USA; Zhenning Yang, University of Tennessee, Knoxville, Knoxville, USA, znyang@umich.edu; Gregory Thomas Croisdale, University of Tennessee, Knoxville, Knoxville, USA, gregtc@umich.edu; Çağdaş KARATAŞ, Microsoft, Seattle, USA, cagdaskaratas@gmail.com; Jian Liu, University of Tennessee, Knoxville, Knoxville, USA, jliu@utk.edu.

---

Permission to make digital or hard copies of all or part of this work for personal or classroom use is granted without fee provided that copies are not made or distributed for profit or commercial advantage and that copies bear this notice and the full citation on the first page. Copyrights for components of this work owned by others than the author(s) must be honored. Abstracting with credit is permitted. To copy otherwise, or republish, to post on servers or to redistribute to lists, requires prior specific permission and/or a fee. Request permissions from permissions@acm.org.

© 2023 Copyright held by the owner/author(s). Publication rights licensed to ACM.

2474-9567/2023/9-ART135 \$15.00

<https://doi.org/10.1145/3610927>

## 1 INTRODUCTION

Cycling has become one of the most popular transportation methods and a good form of exercise over the world, owing to its flexible, convenient, low-cost, and environmental-friendly characteristics. A recent report has shown that the number of cyclists in America has grown to 52 million in 2022, with the global bicycle market size of \$59.33 billion, and it is expected to reach \$92 billion by 2028 [4]. Additionally, immersive indoor cycling has been increasing its popularity in recent years as it brings convenience, fun, and competitiveness. Especially during the pandemic, such a “virtual-world” exercise has gained considerable attention. For instance, Zwift [18], the most popular immersive indoor cycling app, has more than 4 million users by January 2022 [6]. To help cyclists track their training progress, improve training efficiency, and evaluate & optimize training performance, cycling fitness tracking has become essential for providing critical cycling-specific information such as the cadence, riding position, and knee joint angles of the cyclist.

**Prior Cycling Fitness Tracking Systems.** Existing cycling fitness tracking systems can be broadly divided into three categories: (1) *On-body-sensor-based* in which various types of sensors are attached to the cyclist’s body to track riding position [42], joint angles [26], or vital signs (e.g., heart rate and body temperature) [38, 45, 46, 54]; (2) *On-bike-sensor-based* in which sensors are attached to the bike’s wheel hub or crank arm to monitor the cycling cadence and speed [9, 12]; and (3) *Vision-based* in which a camera is placed at the side of the cyclist to track and correct cycling postures [25]. Although aforementioned systems show reasonably good performance in tracking certain fitness metrics, they would either require inconvenient setups (e.g., attaching multiple sensors to knees and chest, which may cause usability problems in practice, or have limited tracking capability (e.g., cycling cadence and speed bike sensors). Additionally, vision-based approaches are limited by lighting conditions, obstacles (e.g., body occlusions), and may raise serious privacy concerns. To circumvent all the aforementioned limitations, in this paper, we aim to shift the sensing paradigm to the bike saddle, which continuously interacts with the cyclist’s hip and legs, to track the user’s cycling fitness in a *low-cost* (less than \$50), *convenient* (non-wearable), *comprehensive* (five fitness metrics), and *fine-grained* (leg-level) manner.

**System Objective and Challenges.** In recent years, e-textile (e.g., fabric, fiber, and yarn) sensing has gained considerable attention [34]. As e-textile sensors offer excellent levels of flexibility and malleability, it has been considered as one of the promising solutions for next-generation wearable devices, such as smart gloves [41] and smart clothes [44]. Existing studies also showed the feasibility of using pressure fabric sensors on chairs/bedsheets for seating/sleeping posture monitoring [33, 39]. However, it is important to note that none of these studies have focused on cycling fitness tracking, which is an emerging area owing to the rapid growth of the cycling community. In this paper, we propose SMARCYPAD, the first fabric-sensor-based smart seat pad to capture the interactions between the cyclist’s hip/legs and the saddle while riding, and further track a set of critical cycling fitness metrics, including *cadence*, *per-leg stability*, *leg strength balance*, *riding position*, and *knee joint angles*. We choose pressure sensors to sense the pressure change on the saddle induced by the gluteal muscle movement during cycling, as well as the varying pressure distribution resulting from different riding positions. We use fabric as the material owing to its comfort and high sensitivity compared with yarn and fiber [34]. However, realizing such a system to track the aforementioned cycling fitness metrics raises several practical challenges:

(1) *Sensing Prototype Manufacturing:* We need to carefully choose the material, manufacture the sensors, design the analog circuit, and implement the sensing prototype all from scratch. We need to ensure the sensing prototype can capture the cyclist’s cycling activity and should be able to maintain stability for long-term usage.

(2) *Cycling Fitness Tracking Using Under-hip Fabric Sensors:* Different from existing studies that require attaching various sensors on the cyclist’s legs and trunk, our system only utilizes fabric sensors under the cyclist’s hip, which can only provide non-directive, coarse-grained fabric sensing data. The mapping between the fabric sensing data with the five cycling-specific metrics is unexplored.

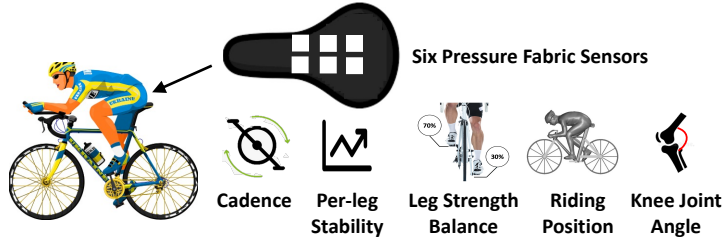


Fig. 1. Estimating five cycling-specific metrics using SMARCyPAD.

(3) *Per-leg Analysis*: To measure leg strength balance and per-leg stability, SMARCyPAD needs to be able to capture the activities of two legs separately. Meanwhile, the sensors should have equal sensitivity for both legs.

**Cycling Fitness Tracking Leveraging Fabric Sensors.** To address these challenges, we propose SMARCyPAD, a smart cycling fitness tracking system in the form of a seat pad, as illustrated in Fig. 1. Specifically, the smart seat pad has six embedded fabric pressure sensors and can be easily deployed on the surface of bike saddles. We utilize two sensing channels to sense the cycling activity of the cyclist's two legs, with each sensing channel composed of three equally-distributed fabric sensors to sense the different pressure distribution caused by different riding positions. The design of the prototype ensures the sensing capability of SMARCyPAD in proving sufficient information to derive the five cycling-specific metrics while maintaining the minimum intrusiveness level to the cyclist. All materials used to build SMARCyPAD are water-proof, reusable, and the total cost is less than \$50. To track the five cycling-specific metrics, we apply static signal processing algorithms to smooth & filter the received sensor signals and further calculate the frequency of the cycling activity and the pedaling time for each leg. The cyclist's cycling frequency is used to derive cadence, while the pedaling time for each leg determines per-leg stability and leg strength balance. Additionally, we train a one-dimensional convolutional neural network (1D CNN) with channel-wise and spatial attention to learn the mapping between the sensor signals and the cyclist's riding position in a supervised manner. Furthermore, to enable the generalizability of SMARCyPAD and further reduce user effort, we apply unsupervised/supervised domain adaption to make the pre-trained CNN model learn cyclist-independent feature representations. Finally, we train a generic linear regressor to continuously track the cyclist's knee joint angle from the sensing data for synchronous leg dynamics reconstruction in virtual scenes. Our main contributions are summarized as follows:

- We propose SMARCyPAD, the first smart seat pad for cycling fitness tracking that can unobtrusively, accurately, and continuously track five cycling-specific metrics including cadence, per-leg stability, leg strength balance, riding position, and knee joint angle.
- We carefully choose the material of the fabric, manufacture the sensors & prototypes all from scratch. Our designated circuit design ensures that the prototypes can accurately capture cycling activities, can be used by cyclists with varying body weights, and maintain stability for long-term usage. The implemented sensing prototype can be used on any bike saddles, with an overall cost of less than \$50.
- We introduce a novel approach to improve the cyclist's immersive experiences and cycling performance. We have developed both signal processing algorithms and deep-learning-networks for processing coarse-grained fabric sensing data in real-time and extracting meaningful insights about the user's cycling body dynamics. Moreover, our algorithms can be generalized to different cyclists with varying body structures and cycling habits.
- Extensive evaluations involving 15 participants demonstrate that SMARCyPAD can estimate the cyclist's cadence with an average error of 1.13 RPM and 1.70% relative error, accurately quantify the per-leg stability, and detect cycling imbalance. Additionally, SMARCyPAD can distinguish five riding positions with an accuracy of 96.60% and can continuously track the cyclist's knee joint angle with an average mean error as low as 9.58 degrees.



Fig. 2. Five riding positions [23].

## 2 PRELIMINARIES

### 2.1 System Objectives for Cycling Fitness Tracking

We aim to derive the following metrics using SMARCYPAD:

**Cadence.** Cadence is defined as Revolution Per Minute (RPM), which directly reflects how fast the cyclist pedals. It is essential for estimating the cyclist's cycling speed and working load. Moreover, maintaining the cadence at an appropriate range (e.g., 80-90 RPM) can help avoid leg fatigue over long training sessions while utilizing energy from slow-twitch muscles [2].

**Per-leg Stability.** Per-leg stability is used to determine whether the cyclist can maintain a relatively stable cycling period under a specific training condition, which is essential for cycling performance evaluation and can help provide suggestions on a personalized training plan. An appropriate training plan would primarily increase training efficiency, while an overwhelming plan could potentially result in injuries.

**Leg Strength Balance.** Leg-strength balance reflects whether the left and right legs apply the same strength. It is essential for diagnosing pedaling asymmetry, which affects cycling performance and increases the risk of knee injuries due to overuse [27]. Moreover, pedaling asymmetry makes cyclists more likely to suffer from premature fatigue during long training sessions because the workload is not spread evenly across the cycling muscles [1].

**Riding Position.** Riding position refers to the cyclist's upper body posture, a correct position can optimize cyclist performance and prevent potential injuries. As illustrated in Fig. 2, our system aims to classify five different riding positions: two types of "back up", "back horizontal", "back down", and "elbow". Existing studies have demonstrated that an appropriate riding position can help reduce the effect of aerodynamic drag and further improve cycling performance [21, 23, 37]. For instance, "back horizontal" is 7.7% faster compared with "back up 2", but 4.7% slower compared with "back down" [23]. Additionally, for indoor virtual cycling, identifying the cyclist's riding position could help reconstruct the cyclist's upper body postures and derive the cyclist's speed more accurately in the virtual scene for a more authentic and immersive experience.

**Knee Joint Angle.** Knee joint angle is the angle between the cyclist's thigh and shank. Additionally, maintaining an appropriate knee flexion angle could help to reduce the maximal power output and prevent knee injuries such as iliotibial band syndrome and chondromalacia [51].

### 2.2 Sensing with Conductive Fabric Sensors

To monitor the aforementioned cycling metrics, we choose to use conductive fabric sensors, which have been widely applied for biomonitoring, rehabilitation, telemedicine, and teleassistance [47]. Specifically, we choose to use pressure fabric (i.e., Velostat [13]), a conductive material made from carbon polyethylene whose resistance drops when external pressure is applied. This pressure-dependent resistance is due to quantum tunneling and percolation [55]. Quantum tunneling affects the conductivity of a composite material when the distance between the conductive particles inside the polymeric material experience deformation (e.g., under pressure), allowing electricity to pass through the material's potential barrier. Additionally, percolation provides a change of conductivity when the applied pressure deforms the contact area of the polymeric material, which changes the

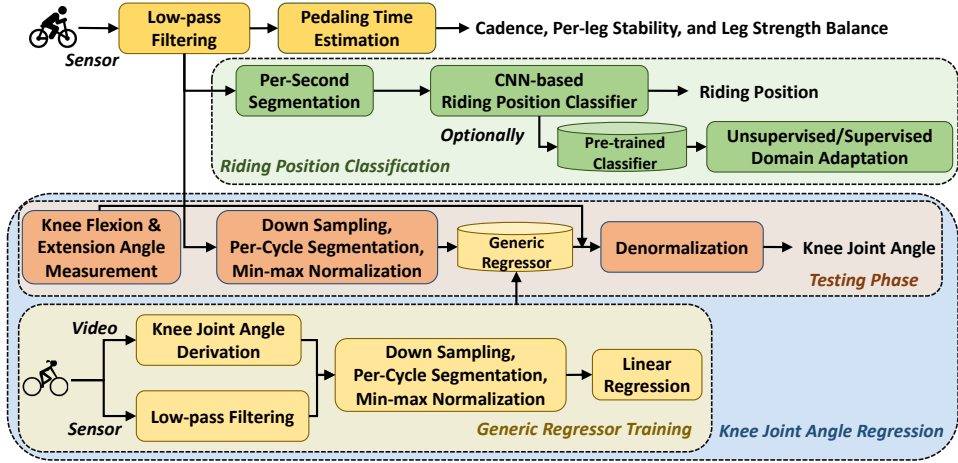


Fig. 3. SMARCyPAD system overview.

conductive paths of the conductive particles [43]. This pressure-sensitive characteristic makes Velostat suitable for sensing the pressure change caused by the cyclist's cycling activities. Moreover, the flexibility and malleability of Velostat make it can be easily customized and deployed on uneven surfaces (i.e., bike seats).

To leverage the properties of Velostat as a variable resistor, we place it between conductive fabrics to create the pressure fabric sensor. Specifically, we utilize the off-the-shelf Faraday fabric [5], which is a polyethylene terephthalate (PET) fabric that incorporates conductive threads of Copper (Cu) and Nickel (Ni) to provide high conductivity and shielding effect. The resistance of the conductive fabric is low, and its shielding band ranges from 10 kHz to 30 GHz, which offers electrical conductivity while also providing the specified shielding effect. In the same way, as with the Velostat, this Faraday fabric offers flexibility and malleability to accommodate non-linear surfaces, making them ideal when working with wearable sensors and sensors that need to be attached to existing surfaces (e.g., seating pads). Furthermore, the Faraday fabric we utilize is non-stretchable woven conductive fabric, allowing it to maintain a relatively stable conductivity and electrical properties (e.g., resistance) [40]. The pressure fabric sensor manufacturing, analog circuit design, and step-by-step prototype manufacturing of SMARCyPAD are detailed in Section 4.

### 3 CHALLENGES & SYSTEM OVERVIEW

#### 3.1 Challenges

**Fabric Sensor and Sensing Prototype Manufacturing:** We need to manufacture the fabric sensors and sensing prototype all from scratch leveraging off-the-shelf materials. We need to ensure the sensors is capable of capturing the cycling activity of the cyclist, and the sensing signal should contain rich information for deriving the five cycling-specific metrics, and can be easily adapted to any bike seats while providing the maximum comfort and convenience level to the cyclist.

**Cycling Fitness Tracking via Under-hip Fabric Sensors.** Different from existing approaches that directly attach sensors on the user's legs and torso, SMARCyPAD only relies on a fabric sensing pad underneath the user's hip. The mapping between the collected coarse-grained fabric sensing data and the user's cycling activity is unknown. Moreover, we aim to derive a comprehensive cycling profile that covers every aspect of the user, including cadence, stability, balance, seating position, knee angle, and trunk angle. Most of these metrics are irrelevant with others, therefore it's challenging to accurately track all of them from the same fabric sensing data.

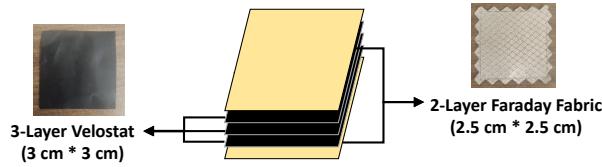


Fig. 4. Structure of the proposed fabric sensor.

**Per-leg Analysis.** SMARCyPAD needs to capture the cycling activity of both legs to estimate per-leg stability and leg strength balance on the limited sensing area of a bike saddle. Additionally, the resistance and sensitivity of the fabric sensors for the two legs should be identical for a fair comparison. However, manufacturing imperfections and asymmetric pelvis structure inevitably result in bias on the sensing signal. We need to design the sensing prototype and our algorithms carefully to mitigate the effect caused by this bias.

### 3.2 System Overview

The overall system structure is illustrated in Fig. 3. We first perform *Low-pass Filtering* on the raw sensor data to remove irrelevant high-frequency components. The filtered signal are then fed into three blocks in parallel: *Cadence, Per-leg Stability, and Leg Strength Balance Estimation; Riding Position Classification; and Knee Joint Angle Regression*. Specifically, we perform *Pedaling Time Estimation* on the filtered sensor signal to get the pedaling time for both legs based on the periodic characteristic of cycling activity. The pedaling time will then be used to derive the cyclist's cadence, per-leg stability, and leg strength balance. Meanwhile, we apply *Per-second Segmentation* to segment the filtered sensor signal into one-second data frames. The segmented frames are then fed into *CNN-based Riding Position Classifier* to learn the mapping between the five riding positions and the sensor signal. Optionally, if the cyclist is not willing to engage in this training phase or can only provide a limited amount of training data, we will prepare a *Pre-trained Classifier*, and SMARCyPAD will adapt the pre-trained classifier to the cyclist's data via *Unsupervised Domain Adaption* or *Supervised Domain Adaption*.

*Knee Joint Angle Regression* contains two sub-blocks: *Generic Regressor Training* in which we recruit a single cyclist to train a generic regressor, and *Testing Phase* in which any cyclist can directly use the generic regressor, without training required. Specifically, the cyclist engaged in the training phase is required to cycle under different riding positions for a certain time period, and we collect both video and sensor data simultaneously. We then perform *Knee Joint Angle Derivation* on the video data to derive the cyclist's knee joint angles using a computer-vision-based approach. We perform the same *Low-pass Filtering* procedure on the sensor data and then perform *Down Sampling, Per-cycle Segmentation, Min-max Normalization* on the filtered sensor data and knee joint angle data synchronously. The normalized sensor signals and the measured joint angle for each cycle are then mapped with each other via *Linear Regression*. In the testing phase, the cyclist first needs to perform a one-time *Knee Flexion & Extension Angle Measurement* to get his/her unique knee flexion & extension angles. The filtered sensor signal passes the same pre-processing procedures in the training phase, and the normalized signal is fed into the *Generic Regressor* to get the normalized knee joint angle. Combined with the previously measured flexion/extension angle, the cyclist's actual knee joint angle can be recovered via *Denormalization*.

## 4 SYSTEM IMPLEMENTATION

In this section, we describe the fabric sensor manufacturing, analog circuit design, and the step-by-step prototyping of SMARCyPAD in detail.

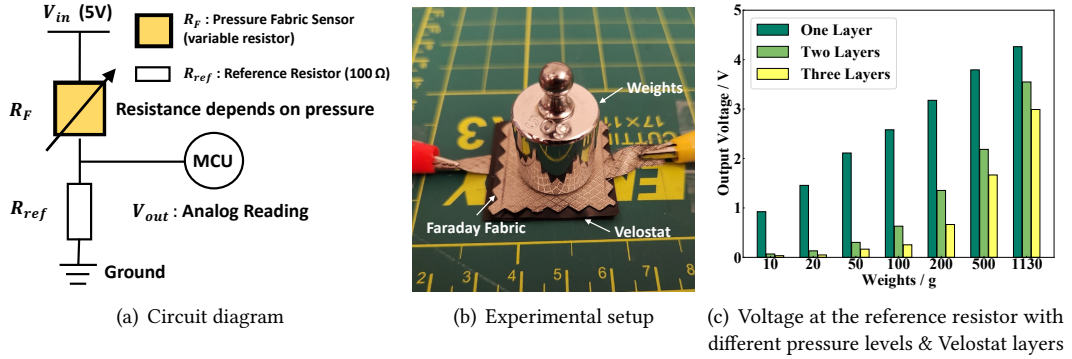


Fig. 5. Sensitivity test of the proposed fabric sensor.

#### 4.1 Fabric Sensor Manufacturing

As discussed in Section 2, the fabric sensor is composed of a Velostat layer placed between two conductive fabric sheets. Specifically, we use three sheets of Velostat to increase resistance, as illustrated in Fig. 4. The size of the Faraday fabric is 2.5 cm by 2.5 cm, and we utilize pinking shear cuts at the side to prevent the fraying of the fabric material. The size of the Velostat is 3 cm by 3 cm, having a larger area compared to the conductive fabric ensures enough space for sewing the Velostat without damaging the sensing areas (detailed in Section 4.3).

**Sensitivity Test.** To test the sensitivity of the proposed fabric sensor, we connect it with a reference resistor  $R_{ref}$  ( $100 \Omega$ ), as illustrated in Fig. 5 (a). The fabric sensor can be regarded as a variable resistor  $R_F$ , whose resistance changes depending on the applied pressure. Given the input voltage  $V_{in}$ , the voltage at the reference resistor  $V_{out}$  can be simply derived as:

$$V_{out} = \frac{R_{ref}}{R_F + R_{ref}} * V_{in}. \quad (1)$$

We then apply different pressure levels to the fabric sensor by adding different weights, as illustrated in Fig. 5 (b). Specifically, we add weights of 10g, 20g, 50g, 100g, 200g, 500g, and 1,133.98g (2.5lb). Moreover, we also test the sensor's sensitivity with different layers of Velostat added between the Faraday fabrics (i.e., one, two, and three layers). The measured  $V_{out}$  is shown in Fig. 5 (c): it is clear to observe that  $V_{out}$  increases as the pressure level increases, which demonstrates  $R_F$  decreases with the pressure level. Please note that the relationship is not linear and the voltage levels start to saturate with increasing weight, which makes the sensor behave as a switch if pressed past its limits. More sheets of Velostat increases the resistance across the Velostat layer hence enabling a broader range of sensitivity compared with fewer layers thus increasing the weights the sensor can operate without saturating. When there is only one layer of Velostat, 2.5 lb of weight can increase  $V_{out}$  up to 4.26 V, while the increased voltage is only 2.99 V with three layers, indicating the sensor can endure a higher level of pressure. Thus, three layers of Velostat between the Faraday fabric are used in SMARCYPAD.

#### 4.2 Analog Circuit Design

The overall circuit schematic of SMARCYPAD is illustrated in Fig. 6 (a). To reduce the computational overhead, we utilize two identical channels to sense the cycling activity, with one channel per leg. Each channel is composed of two circuit stages: voltage divider stage and analog reading stage. Each circuit stage is manufactured in a corresponding physical layer. Four zigzag-shaped long conductive threads with  $R_T$  resistance connected in series with Vcc and Ground pins create the voltage divider layer. Due to the limited space on the saddle and the required

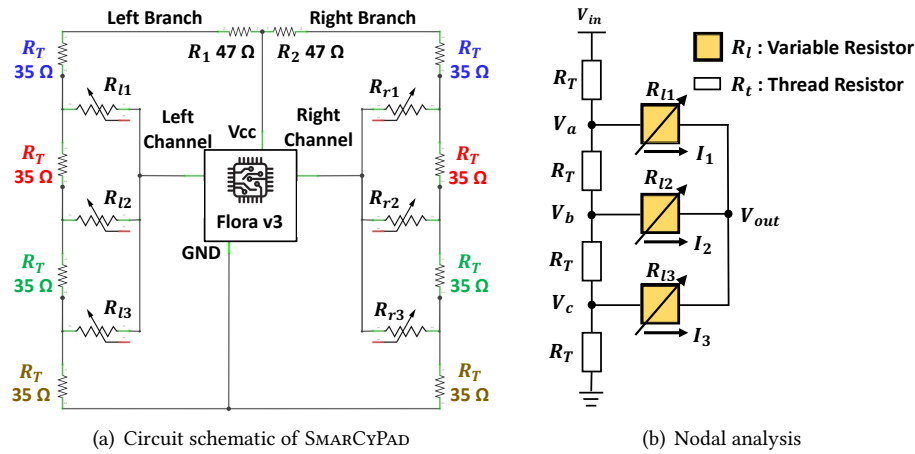


Fig. 6. Circuit schematic of SMARCPAD.

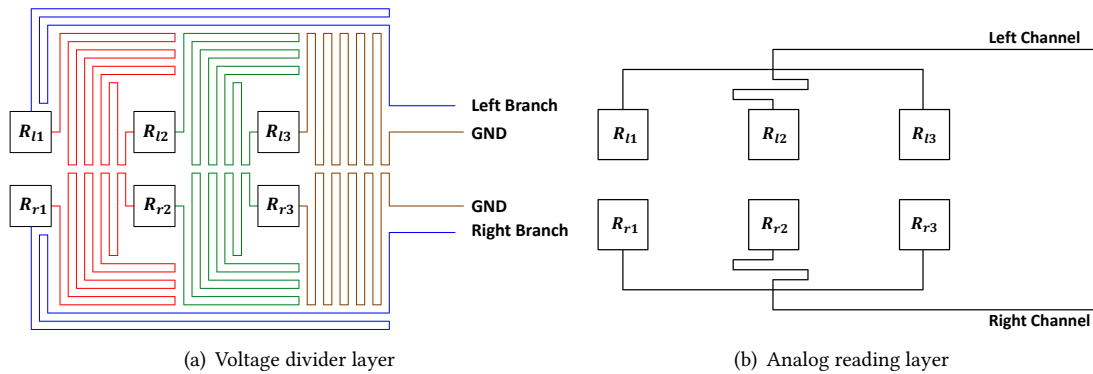


Fig. 7. Diagram of the conductive threads.

zig-zag pattern for the conductive thread, the analog reading stage contains three fabric sensors to capture the pressure distribution ( $R_{l1}, R_{l2}, R_{l3}$  for the left channel, and  $R_{r1}, R_{r2}, R_{r3}$  for the right channel). Each sensor is connected to a different stage of the voltage divider and to a common sensing line. The sensing lines are then connected to the analog input pins of the Micro Controller Unit (MCU). Hence the voltage measurements at analog pins are a combination of voltage divider levels and sensor resistance. Therefore, the MCU measurement is affected by the pressure applied to the sensors. This allows us to infer the pressure distribution from the MCU voltage readings.

We conduct nodal analysis on the left channel of SMARCPAD by utilizing Kirchhoff's Current and Ohm's Laws. Given that the input impedance of the MCU is much higher than the overall resistance of the circuit, the nodal analysis diagram is represented as in Fig. 6 (b). The voltage that would enter the ADC reading pin for the MCU  $V_{out}$  can be formulated as:

$$V_{out} = \frac{V_a R_{l2} R_{l3} + V_b R_{l1} R_{l3} + V_c R_{l1} R_{l2}}{R_{l2} R_{l3} + R_{l1} R_{l3} + R_{l1} R_{l2}}. \quad (2)$$

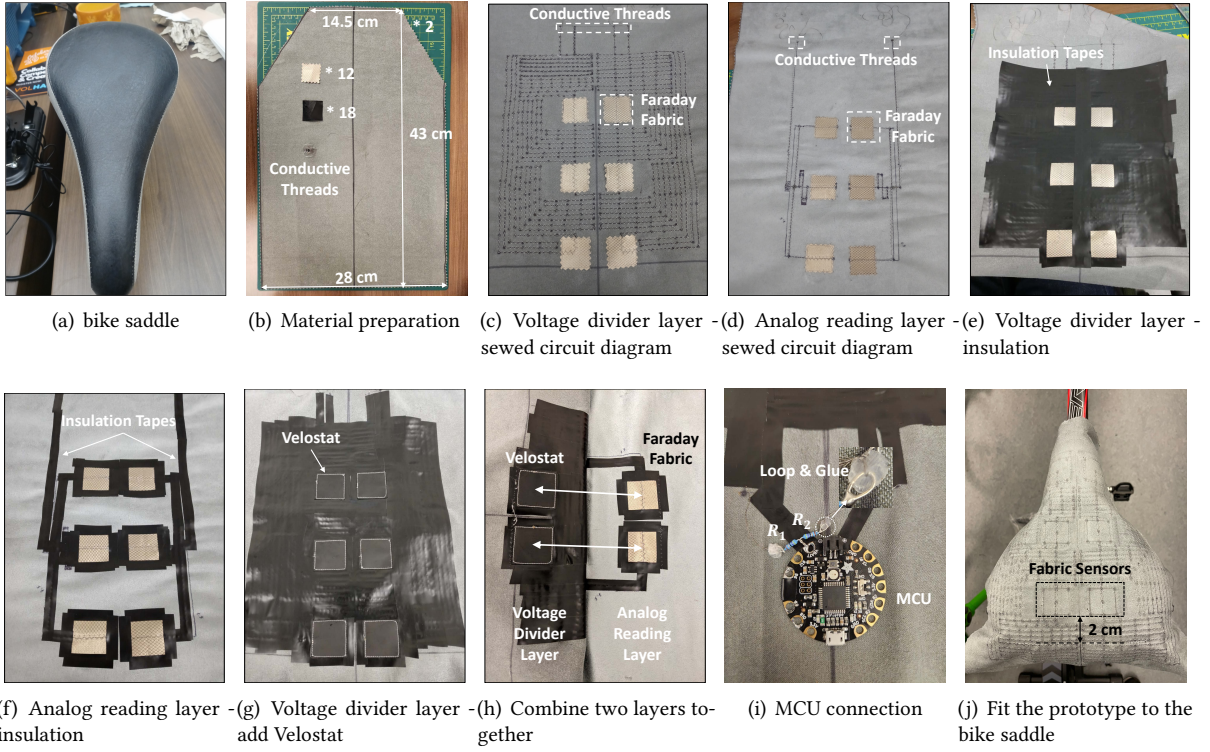


Fig. 8. Step-by-step prototype manufacturing of SMARCYPAD.

When the pressure is applied to  $R_{l1}$ , its resistance will largely drop, making  $V_{out}$  closer to  $V_a$ . Similarly, applying pressure to  $R_{l2}$  and  $R_{l3}$  will get  $V_{out}$  closer to  $V_b$  and  $V_c$ , respectively. Considering that  $V_a$  is greater than  $V_b$  and  $V_b$  is greater than  $V_c$  due to their respective voltage drop across the thread resistance  $R_T$ , applying pressure to different sensors will result in different voltage readings, making SMARCYPAD able to capture the pressure distribution on the saddle.

**Voltage Divider Layer.** The voltage divider layer contains all the  $R_T$  between pressure sensors, formulated by the conductive threads' resistance. The diagram of the threads is illustrated in Fig. 7 (a). Different colors of lines correspond to the  $R_T$  labeled using the same color in Fig. 6. We use the zigzag pattern to maximize the overall length of the threads for a higher resistance, which could help to increase the sensing range of SMARCYPAD. The length of all the thread segments is 90 cm, which ensures that all  $R_T$  is 35  $\Omega$ . Moreover, each branch is connected with a 47  $\Omega$  reference resistor and further connected to the voltage input of the MCU at one end, while the other side is connected to the ground pin of the MCU.

**Analog Reading Layer.** The analog reading layer is connected to the bottom layer of Faraday fabrics and is in charge of sending the voltage change readings of both channels to the MCU. Fig. 7 (b) details the diagram for the conductive thread, which follows a parallel configuration to cover all the pressure sensors. We use an Adafruit FLORA v3 MCU [8] to provide the input voltage and convert the analog sensor readings into digital signals.

#### 4.3 Step-by-step Prototyping

**Materials Preparation.** Fig. 8 (a) illustrates a bike saddle which exhibits a commonly-seen triangular shape. SMARCYPAD is shaped in a way to cover the bike saddle as shown in Fig. 8 (b). Specifically, the total length of the

saddle pad is 43 cm, with a width of 14 cm at the shorter end and 28.5 cm at the longer end. We use suede as the material of the seat pad due to its non-conductive properties, durability, softness, and lightness [14]. We cut two pieces of suede which represents the two layers; one holds the voltage divider layer while the other holds the analog reading layer. Following the shape and size illustrated in Fig. 4, we then manufacture 18 pieces of Velostat and 12 pieces of Faraday Fabric for the 6 fabric sensors. We use conductive threads [16] as cables to connect everything together. The materials listed above are all water-proof and washable [17].

**Circuit Diagram Sewing.** The circuit diagram in Fig. 7 is printed on a tracing paper and further traced on the suede. The voltage divider and the analog reading layers are traced on the two suede pieces, respectively. We then stick the six pieces of Faraday fabric into the sensing areas in the diagram for both layers. Specifically, we add iron-on hem tape [11] between the suede and the Faraday fabric and utilize a Dritz 29500 Petite Press Portable Mini Iron [7] to heat the Faraday fabric. The hem tape is then melted and sticks the Faraday fabric with the suede. The conductive threads are sewed on the suede following the traced circuit diagram using a 4411 Heavy Duty Singer sewing machine [15]. The zigzag sewing pattern has a width of 3 and a length of 2.2, which helps to maintain our predetermined resistance characteristics. Additionally, we leave approximately 30 cm of conductive thread at the beginning and end of the diagram for the connection with MCU. The sewed diagram, along with the embedded Faraday fabrics for the two layers, are shown in Fig. 8 (c) and (d), respectively.

**Insulation and Addition of Velostat.** To prevent the contact of conductive threads which will result in short circuit, insulating tape is used to cover exposed areas of conductive threads except for the six sensing areas for each layer, as shown in Fig. 8 (e) and (f). Note the electrical tape is attached to the inner side of the prototype, ensuring that it does not come into contact with the user's body and affect their comfort while sitting on the seat. Once the insulation is complete, the Velostat is added. The Velostat pieces are added utilizing non-conductive threads to the voltage divider layer, as shown in Fig. 8 (g). Since the Velostat pieces are slightly larger than the conductive fabric sensing areas, we lay the three layers of Velostat to the suede and provisionally attach them with tape while ensuring the complete coverage of the sensing areas. Finally, we sew the Velostat pieces on the suede along their edges while ensuring no additional pressure is applied, which can affect their resistivity characteristics.

**Wrap Up.** By this point, we have two layers of suede: voltage divider layer with exposed Velostat, and analog reading layer with exposed Faraday fabric. As illustrated in Fig. 8 (h), we stack the two layers together to form the final prototype of SMARCPAD. Specifically, the analog reading layer is placed on the bottom, with the voltage divider layer lying on top of it. We use non-conductive threads to sew the two layers together and ensure each Faraday fabric on the analog reading layer is strictly aligned with its corresponding Velostat at the voltage divider layer. The Velostat is thus embedded between two layers of Faraday fabric, formulating the structure in Fig. 4. The final step is to connect  $R_1$ ,  $R_2$ , and MCU to the prototype. As shown in Fig. 8 (i), we solder  $R_1$  and  $R_2$  in parallel to the battery output pin of the MCU. We fix the MCU on the vertical center line of the voltage divider layer, approximately 6 cm away from the sewed diagram. The conductive threads of the left branch, right branch, and grounds, are connected to  $R_1$ ,  $R_2$ , and the ground pin on the MCU, respectively. The end of  $R_1$  and  $R_2$  are made in a loop shape and welded to prevent the conductive thread from coming loose. We then knot the conductive thread with the resistor loop and use a hot glue gun to glue, insulate, and keep the knot from detaching, as illustrated in Fig. 8 (i). Finally, we knot and glue the two analog reading lines from the analog reading layer to the MCU's analog reading pins for the left and right channels. As common bike saddles share similar sizes (135-160mm) [3], we standardized the sensor placement for all saddles by placing the last two sensors 0.75 inches away from the end of the saddle, as illustrated in Fig. 8 (j).

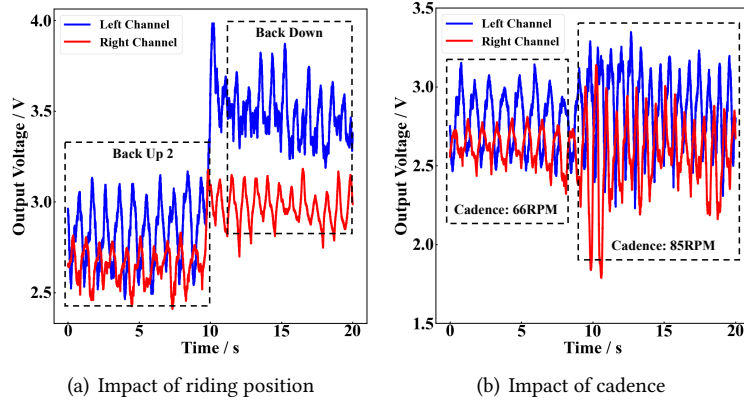


Fig. 9. Two-channel fabric sensing signal during cycling with different riding positions/cadence.

#### 4.4 Feasibility Test

To validate whether the developed SMARCYPAD can sense cycling activities, we conduct a feasibility test where one cyclist is asked to cycle with different cadence (i.e., 66 RPM and 85 RPM) and riding positions (i.e., back up 1 and back down), and the measured sensor signal is illustrated in Fig. 9. The experimental setup is the same as Fig. 8 (j). We observe the two-channel sensor readings clearly reflect the periodic moving patterns for the two legs, with a faster speed indicating a more frequent pressure change. Additionally, the change of pressure distribution caused by different riding positions is also reflected on the voltage reading. For instance, when the cyclist changes the riding position from “back up 1” to “back down”, his/her body would lean more forward and puts more pressure on the front part of the seat (i.e., more pressure on  $R_{l1}$ ), therefore decreasing the resistance at a larger scale and further increase the voltage reading. Additionally, we recruit cyclists with varying body weights to test the sensing range of SMARCYPAD. Specifically, while the cyclists is cycling using the “back down” position which induces the largest pressure, a 95 kg cyclist will increase the voltage up to 4.39 V, which is sufficiently within the maximum sensing range (i.e., 5V). These observations confirm the sensing capability of SMARCYPAD.

### 5 CYCLING FITNESS TRACKING LEVERAGING FABRIC SENSING

In this section, we describe the detailed procedure of deriving the five cycling-specific metrics from the sensing signals. The raw sensor readings first pass through a low-pass filter to remove cycling-irrelevant high-frequency noises. As the RPM for regular cycling is mostly lower than 120 (i.e., 2 cycles per second), we apply a butterworth low-pass filter with order 5 and cutoff frequency of 3 Hz. The filtered sensing signal are then fed into three different blocks, as mentioned in Section 3.2.

#### 5.1 Cadence, Per-leg Stability, and Leg Strength Balance Estimation

**Pedaling Time Estimation.** As cycling activities will formulate a periodic pattern on the sensing signals, we apply a peak detection algorithm provided by the Scipy toolkit [57] to detect each cycle period. We empirically regulate the distance between two adjacent peaks to be at least 0.5 seconds and the prominence (i.e., the minimum distance between the peak and its lowest contour line) to 0.2 V for both channels. The detected peaks are marked using red dots in Fig. 10, with two adjacent peaks forming a single pedaling period. Additionally, a single pedaling time can be divided into two parts: left-leg pedaling and right-leg pedaling. While the cyclist is pedaling using one of the legs, the pressure exerted by the gluteal muscles increases and lowers the sensor’s resistance on

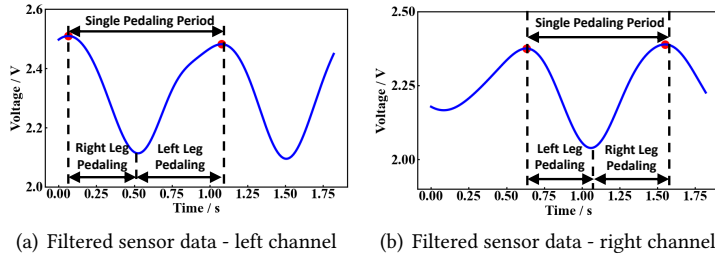


Fig. 10. Pedaling time estimation.

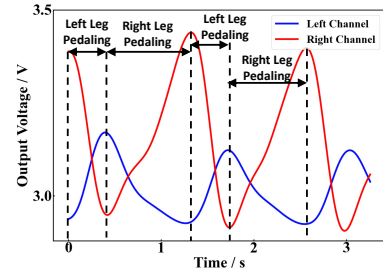


Fig. 11. An example of imbalanced cycling.

the corresponding channel, increasing the voltage reading. As illustrated in Fig. 10 (a), for the left channel, the ascending part in a single pedaling period indicates left leg pedaling and the descending part indicates right leg pedaling, while it is vice versa for the right channel, as illustrated in Fig. 10 (b). Therefore, for each cycling period in each channel, we get the whole pedaling time  $t$ , the left-leg pedaling time  $t_l$ , and the right-leg pedaling time  $t_r$ .

**Cadence Estimation.** We calculate the average pedaling time for each cycle  $\bar{t}$  using the two-channel data, and the cadence of the cyclist can be simply derived as  $\frac{60}{\bar{t}}$  RPM (Revolutions per Minute).

**Per-leg Stability Estimation.** We use *Root Mean Square of Successive Differences* (RMSSD) to quantify the per-leg stability. RMSSD is originally used to measure the heart rate variability as it reflects the beat-to-beat variance of the patient, which can be used to detect the fluctuation in the heartbeat [50]. Similarly, we use it to measure the pedaling time variability and detect whether the cyclist is able to maintain a stable training process. For each leg, given the difference between adjacent pedaling time as  $\Delta t$ , RMSSD is derived as

$$RMSSD = \sqrt{\frac{1}{n-1} \sum_{i=1}^n \Delta t^2}, \quad (3)$$

where  $n$  is the total number of cycling periods. A larger RMSSD indicates a larger variance between the successive pedal and a more unstable cycling process.

**Leg Strength Balance Estimation.** *Asymmetry Index* (AI) is used to quantify the leg strength balance. Given the average pedaling time of the left leg and right leg calculated using both channels as  $\bar{t}_l$  and  $\bar{t}_r$ , AI is calculated as  $AI = \frac{\bar{t}_l - \bar{t}_r}{(\bar{t}_l + \bar{t}_r)/2}$ . As the cycling resistance is the same for both legs, we assume a shorter pedaling time indicates a larger force. Therefore, a negative value of AI means the average pedaling time for the left leg is shorter, indicating the left leg applies more force, while a positive value means the right leg applies more force. Meanwhile, a larger absolute value of AI indicates a higher imbalance level.

Note that we do not directly use the pressure readings to determine the balance of the cyclist. Balance can be determined through the force exerted on the pedal, whereas the pressure reading can only reflect the force exerted by gluteal muscles on the saddle, and cannot directly determine the balance as other factors, such as the cyclist's sitting position, and leaning direction may also affect the sensor readings. Fig. 11 illustrates an example in which the cyclist is cycling only using the left leg. We can observe that the pressure reading for the right leg is higher than the left leg possibly due to the factors such as body leaning direction. However, the left leg has a significantly shorter pedaling time, which suggests that more force is exerted on the left leg.

## 5.2 Riding Position Classification

**Per-second Segmentation.** The filtered sensor data is segmented into one-second frames with no overlaps, which serve as the input of the CNN-based classifier. The sampling rate of the sensor is set to 1200 Hz, making the shape of the data frame (2 \* 1200).

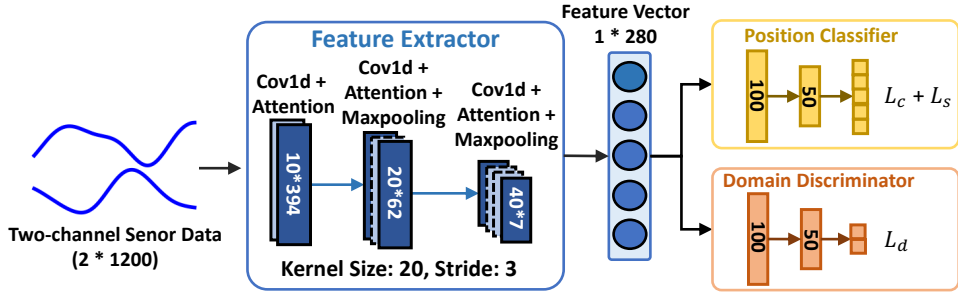


Fig. 12. 1D CNN-based riding position classification network.

**CNN-based Riding Position Classifier.** The structure of the riding position classification network is illustrated in Fig. 12. The input is one-second two-channel sensor data frames, and the output is the probability of five riding positions. The network contains two components: a 1D CNN-based feature extractor that extracts high-level feature representations from the sensor data and a fully connected layer-based position classifier that classifies the position from the feature vector. Specifically, the feature extractor contains three 1D convolutional layers with kernel size set to 20 & stride set to 3 and two max-pooling layers with the kernel size set to 2. Additionally, we add Convolutional Block Attention Module (CBAM) [60] after each convolutional layer, refining the feature representations via the channel and spatial attention. Specifically, channel- and spatial-wise attention calculates the inter-channel and inter-spatial relationship of the features, and larger weights are assigned to more critical parts. The output shape of the last layer is  $40 * 7$  and further flattened to a  $1 * 280$  feature vector. The position classifier contains three fully-connected layers with 100, 50, and 5 neurons. We utilize cross-entropy as the loss function. The network is trained using the Adam optimizer, with the learning rate set to 0.001. Each layer is followed by a batch normalization layer to speed up and stabilize the training process through mitigating internal covariate shift [32] and has a dropout rate of 0.2 to avoid over-fitting.

**Unsupervised Domain Adaptation.** Cyclists are required to involve in a training phase to get the cyclist-dependent riding position classifier. However, certain users may intend to skip this part for quick enrollment, for which we would prepare a pre-trained classifier. Nevertheless, cyclists vary a lot in body weight and structure, making the sensor readings for each individual have a unique pattern. As the pre-trained model's robustness largely relies on the training data, its performance will inevitably decrease if the data is unseen in the training phase. To address this problem, we fine-tune the pre-trained classifier via unsupervised domain adaptation [29] to make it learn domain-independent feature representations. Here different cyclists are domains, and we aim to make the pre-trained model can be generalized to the testing cyclist (i.e., target domain) from the training cyclist (i.e., source domain). As illustrated in Fig. 12, we add an additional domain discriminator with three fully connected layers after the feature extractor, which aims to distinguish whether the sensor data is from the source domain or target domain. We use binary cross entropy as the loss function for the domain discriminator. Given the loss of the position classifier as  $L_c$  and the domain discriminator as  $L_d$ , the loss of the whole network  $L$  is formulated as  $L_c - \lambda L_d$ , in which we minimize the loss of the position classification while maximizing the loss of the domain classification.  $\lambda$  indicates the weight of the domain discriminator, which is set to 2. The feature extractor can then learn to extract representations that are generalized among different cyclists to improve the robustness of the pre-trained classifier.

**Supervised Domain Adaptation.** Additionally, if the cyclist can provide a limited amount of labeled data (approximately 1 minute in total), we can utilize supervised domain adaptation [56] to fine-tune the pre-trained classifier. In practice, obtaining this amount of labeled data should be a straightforward task. The cyclist can simply engage in a brief warm-up exercise prior to using our system following a set of instructions to perform

different riding positions in a pre-defined order. Similar to the process of unsupervised domain adaptation, all available labeled data will be fed into the position classifier, while a domain discriminator will distinguish the domain of the data. However, in addition to this, we incorporate a soft label loss function ( $L_s$ ), which compares the probability distribution for each labeled sample in the target domain with samples belonging to the same class in the source domain. The loss is thus formulated as  $L_c + \alpha L_s - \lambda L_d$ , and we set  $\alpha$  to 0.5 and  $\lambda$  to 2.

### 5.3 Knee Joint Angle Regression

**5.3.1 Generic Regressor Training.** The generic regressor is trained on a single participant in this work.

**Knee Joint Angle Derivation.** During training, a camera is placed on the cyclist's left side to capture body movement. The frame rate of the recorded video data is fixed at 30. To derive the knee joint angle, we first detect the body skeleton of the cyclist in each video frame via OpenPose [24], a real-time system that can detect the coordinates of 25 human body keypoints on single images. Fig. 13 illustrates the detected skeleton while the cyclist is cycling, and we only preserve 3 of these keypoints: the hip, knee, and ankle. Given the combinations of these three keypoints as  $\{k_1, k_2, k_3\}$ , the knee joint angle of the cyclist  $\theta_k$  can be easily derived as

$$\theta_k = \arccos\left(\frac{\overrightarrow{k_1k_2} \cdot \overrightarrow{k_2k_3}}{|\overrightarrow{k_1k_2}| |\overrightarrow{k_2k_3}|}\right). \quad (4)$$

**Data Pre-processing.** We first down-sample the filtered sensor data to make its sampling rate consistent with the joint angle data. We ensure the sensor data and the angle data are strictly synchronized, then perform the peak detection algorithm on the sensor data the same way as mentioned in Section 5.1. Both sensor data and angle data are then sliced according to the detected peaks, with two adjacent peaks forming a data segment. Additionally, to eliminate the cyclist- and riding-position-dependent characteristics, for each data segment, we utilize min-max normalization on both joint angle and sensor data to make them within the range from 0 to 1.

**Linear Regression.** We observe the Pearson Correlation Coefficient (PCC) between the normalized sensor data and knee joint angle reaches 87.82%, indicating a high linear correlation. We thus apply standard linear regression provided by Scikit-learn [48] to map them together. As the knee joint angles for the two legs follow an alternative pattern, we only train the regressor for the left leg, and the joint angle of the right leg is then derived from the left leg's angle. Given the sensing data  $s_t$  and knee joint angle  $\theta_t$  at timestamp  $t$ , we linearly define their relationship as  $\theta_t = As_t + B$ . We combine all the normalized data segments and train the standard linear regressor.

In addition to the linear regressor, we also test the performance of quadratic and cubic regressors. We observe a slightly worse performance: on the training set, linear regressor reaches an average error of 5.95 degrees, while quadratic/cubic regressors result in 6.43/6.48 degrees. Moreover, the inference time for the linear regressor (0.0025 ms) is much shorter compared with quadratic/cubic regressors (0.0042/0.0061 ms). We thus model the relationship between sensor reading and knee joint angle using linear regression.

**5.3.2 Testing Phase.** In the testing phase, any cyclist can directly use the pre-trained generic regressor for continuous knee joint angle reconstruction without requiring any training efforts. Specifically, the left-channel sensor data passes through the same pre-processing procedures as in the training phase and is then fed into the generic regressor to get the normalized knee joint angle for the left leg.

**Knee Flexion & Extension Angle Measurement.** Before starting cycling, the cyclist is required to perform a one-time knee flexion/extension angle measurement. As illustrated in Fig. 13 (a), the flexion angle  $\theta_f$  is the maximum knee joint flexion, while the extension angle  $\theta_e$  is the maximum knee joint extension, as shown in Fig. 13 (b). We assume they remain the same for both legs throughout the cycling activity.

**Denormalization.** Given the normalized knee joint angle of the left leg is  $\theta_l$ , the normalized knee joint angle of the right leg is calculated as  $1 - \theta_l$ , following the alternative characteristic. With the measured  $\theta_e$ ,  $\theta_f$ , and



(a) Knee flexion angle measure-  
ment (foot and pedal at the high-  
surement (foot and pedal at the  
est point, knee flexing)  
(b) Knee extension angle mea-  
surement (foot and pedal at the  
lowest point, knee extending)



Fig. 13. Knee joint angle derivation and extension/flexion angle measurement.

Fig. 14. Saddles used for evaluation.

normalized angle  $\hat{\theta}$ , the actual knee joint angle of the cyclist  $\theta$  can be derived through denormalization:

$$\theta = (\hat{\theta} + \theta_f) \times (\theta_e - \theta_f). \quad (5)$$

## 6 PERFORMANCE EVALUATION

### 6.1 Experimental Methodology

**Experimental Setup & Data Collection.** We recruit 15 cyclists (C1 to C15) to evaluate the performance of SMARCYPAD. The cyclists include 11 males and 4 females aged from 20 to 34. The height of these cyclists varies from 5' 3" to 6'1", and their body weights range from 103 to 210 lbs. We have deployed SMARCYPAD on three bike saddles with different shapes & sizes, as shown in Fig. 14: the saddle of a TREK Domane AL 2 road bike (S1), BLUEWIND Bike Seat (S2) [19], and Wittkop Bike Seat (S3) [20], which all have received numerous ratings on Amazon. The sampling rate of the fabric sensor is fixed at 1200 Hz. To evaluate the performance of cadence estimation, riding position classification, and knee joint angle regression, each cyclist is asked to cycle for 15 minutes using the five different riding positions illustrated in Fig. 2, with each position lasting for 3 minutes. A camera is placed on the cyclist's left side to measure their knee joint angle and cadence. The participants adjust the bike seat height, cycling speed, and working load in their most comfortable way. Before the experiments, we take two photos at maximum knee flexion/extension to measure the cyclist's knee flexion/extension angles. All 15 cyclists conduct experiments on S1, while 5 cyclists are recruited for experiments on S2 and S3. Cyclists are required to complete a questionnaire on their experience with SMARCYPAD after data collection.

For the evaluation of per-leg stability estimation, we recruit five cyclists and ask them to cycle at different speeds (i.e., 10 mph and 15 mph), each lasting for five minutes. After the experiment, they are required to provide a difficulty rating of maintaining certain speeds within the range from 1 to 5, with 1 indicating "very easy" and 5 standing for "very hard". Finally, the five cyclists are asked to cycle only using the left leg for three minutes and then only using the right leg for another three minutes. The imbalanced pedaling data will be used to evaluate the performance of leg strength balance estimation. In total, we have collected around 900 mins of cycling data from 15 participants, containing around 94,500 riding cycles, over a ten-month period to evaluate the performance of SMARCYPAD<sup>1</sup>.

<sup>1</sup>The study has been approved by our Institutional Review Board (IRB).

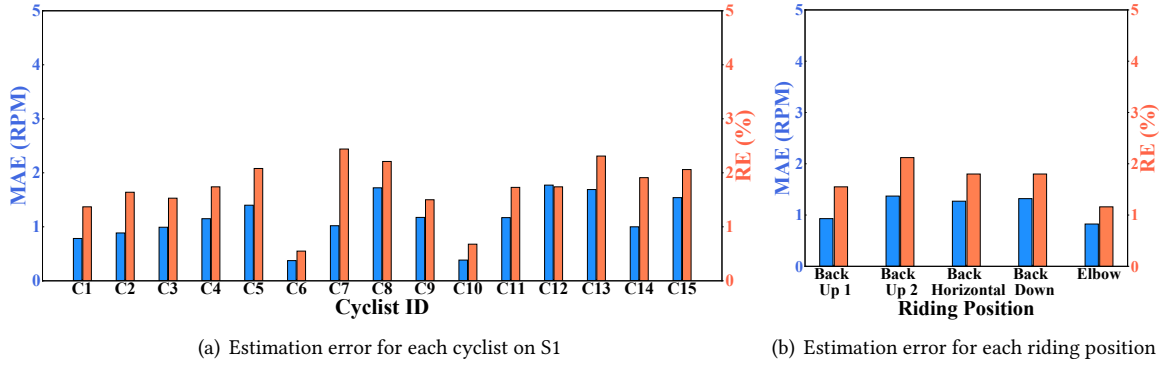


Fig. 15. Performance of cadence estimation.

**Evaluation Metrics.** We use the following metrics to evaluate the capability of SMARCYPAD in tracking various fitness metrics: (1) *Mean Absolute Error (MAE)* and *Relative Error (RE)* are used to evaluate the performance of cadence estimation. MAE is calculated as  $MAE = ||g - e||$  and RE is calculated as  $RE = \frac{||g - e||}{g}$ , in which  $g$  and  $e$  represents the groundtruth and estimated cadence; (2) *Accuracy, Precision, and Recall* are used to evaluate the performance of riding position classification. Accuracy is defined as the percentage of correctly classified positions among all positions, the precision of the  $i$ th position is defined as  $\frac{TP_i}{TP_i + FP_i}$ , and the recall of the  $i$ th position is defined as  $\frac{TP_i}{TP_i + FN_i}$ , where  $TP_i$ ,  $FP_i$ ,  $FN_i$  are the true positive rate, false positive rate, and false negative rate for the  $i$ th position, respectively; and (3) *MAE* is used to evaluate the performance of knee joint angle regression. In addition, we also use *Pearson Correlation Coefficient (PCC)* to calculate the linear correlation between the reconstructed knee joint angle series with the ground truth captured by the camera.

## 6.2 Performance of Cadence, Per-leg Stability, and Leg Strength Balance Estimation.

**6.2.1 Cadence Estimation.** Fig. 15 (a) illustrates the average MAE & RE of the estimated cadence for each cyclist on S1. We find that all cyclists achieve comparable low errors. The average MAE for all cyclists is only 1.13 RPM and RE is 1.70%. C6 achieves the lowest error among all cyclists with 0.37 MAE and 0.55% RE, with all cyclists' MAE lower than 2 RPM and RE lower than 2.5%. The average error of the ten cyclists for each position is illustrated in Fig. 15 (b). Similarly, we observe comparable low errors for all riding positions. “Elbow” achieves the best performance with only 0.6 MAE and 0.82% RE, and all positions have a RE lower than 2.5%. As the cadence of the cyclists varies from 41 to 112 RPM, the promising results demonstrate that SMARCYPAD can accurately measure the cyclist's cadence and is robust to different cycling speeds & riding positions.

**6.2.2 Per-leg Stability Estimation.** Fig. 16 (a) and (b) illustrate the calculated RMSSD while the participants are cycling at two different speeds, along with their difficulty rating in maintaining the specific speed. We observe that our measured RMSSD achieves high consistency with the cyclist's difficulty ratings. Specifically, all participants feel it is relatively easy to maintain the speed at 10 mph, and the corresponding RMSSD is also low. Meanwhile, the two participants that give a “Very Easy” rating achieve a lower RMSSD compared with others that give a “Easy” Rating. However, all cyclists give 15 mph a “Hard” rating over 4, and the RMSSD also increases accordingly. Fig. 17 (a) and (b) visualize the whole experimental process of C1 using the moving variance of the pedaling time with the sliding window size set to 10 seconds. It is clear to observe that when the speed is 10 mph, the moving variance of the pedaling time is relatively slight and steady, indicating stable cycling progress and the cyclist could consider to increase the workload/speed. However, when the target speed rises to 15 mph, the participant

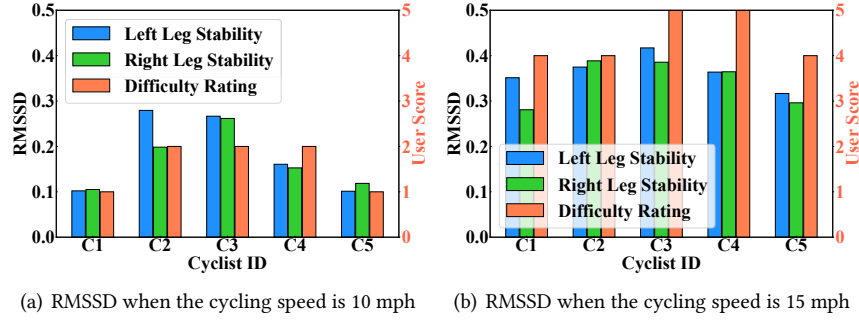


Fig. 16. Performance of per-leg stability estimation.

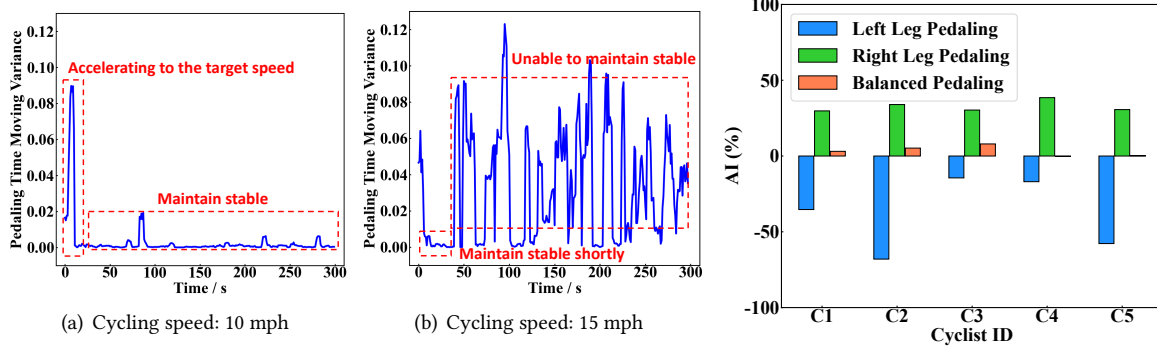


Fig. 17. Moving variance of the pedaling time.

Fig. 18. Performance of leg strength balance estimation.

can only maintain stable cycling for a short period, then the moving variance of pedaling time starts fluctuating acutely, indicating the current training plan is too constrained for the cyclist and results in a larger RMSSD. The measurement results demonstrate that SMARCYPAD is capable of quantifying the per-leg stability of the cyclist and provide personalized suggestions to the cyclist's training plan.

**6.2.3 Leg Strength Balance Estimation.** The calculated AI of the five participants, when they were cycling using the left leg, right leg, and both legs are illustrated in Fig. 18. We observe that SMARCYPAD can accurately detect cycle imbalance. Specifically, all cyclists achieve a negative value of AI when the left leg puts more strength, while a positive value is derived when the right leg puts more strength. Additionally, balanced cycling shows a significantly smaller absolute value compared with imbalanced cycling, indicating the strength applied by both legs is relatively similar. The promising results demonstrate the capability of SMARCYPAD on estimating the cyclist's leg strength balance and detecting imbalance pedaling.

### 6.3 Riding Position Classification

**6.3.1 Cyclist-dependent Scenario.** We first evaluate the performance in the cyclist-dependent scenario in which the training, validation, and testing data come from the same cyclist. For each cyclist, we divide the whole dataset into three parts: training data, validation data, and testing data with a ratio of 3:1:1. The model exhibiting the best performance on the validation set is deployed to the testing set for performance evaluation. The accuracy,

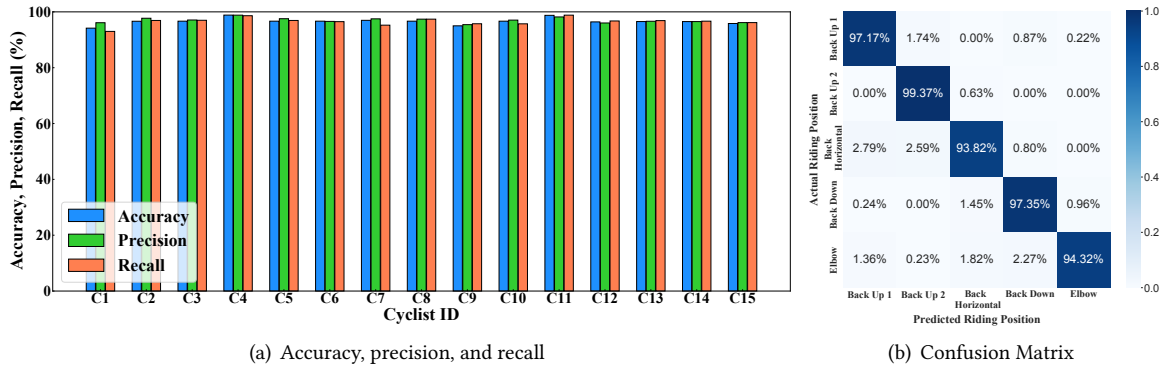


Fig. 19. Performance of riding position classification - cyclist-dependent scenario.

precision, and recall for each cyclist are illustrated in Fig. 19 (a), with an average of 96.10%, 96.53%, and 95.06%, respectively. We achieve an average accuracy, precision, and recall of 96.60%, 96.98%, and 96.55% on the validation set, which is comparable with the testing set. C11 has the best performance with 98.76% accuracy, while the cyclist with the worst performance still achieves 90.28% accuracy. The confusion matrix is illustrated in Fig. 19 (b); we observe that all five positions can be distinguished with an accuracy over 93.82%. The promising results demonstrate the effectiveness of SMARCyPAD on riding position classification.

**6.3.2 Cyclist-independent Scenario.** We further evaluate the robustness of SMARCyPAD in the cyclist-independent scenario, in which no labeled data or only one-minute data is available during training. For each cyclist, all other cyclists' data is utilized in the training phase. The performance on S1 is illustrated in Fig. 20. We observe without domain adoption, we can only achieve an average accuracy of 49.09%, as the sensing signal varies largely from different individuals. However, the average accuracy largely increases to 77.67% with unsupervised domain adaptation, with an average performance gain of 28.52%, demonstrating the effectiveness of unsupervised domain adaptation. Moreover, with only one-minute labeled data, the average accuracy can boost up to 92.97%, which is nearly comparable with the cyclist-dependent scenario. The confusion matrix for supervised domain adaptation is illustrated in Fig. 20 (b); we observe all positions can be distinguished with an accuracy over 90.57%, indicating SMARCyPAD can detect the cyclist's position with high accuracy even if only few labeled data is available.

**6.3.3 Impact of Training Data Size.** We further evaluate the robustness of SMARCyPAD with different training data sizes to explore whether the training effort can be further reduced. Fig. 21 illustrates the performance of riding position classification when the training data size is set to 5, 9, 12, and 14 minutes. We observe when the training data size is decreased to five minutes, SMARCyPAD achieves an average accuracy, precision, and recall of 94.59%, 93.84%, and 92.97%; with 14 minutes of training data, the accuracy, precision, and recall can be increased to 98.39%, 98.56%, and 98.71%. A larger training data size leads to a better performance, but SMARCyPAD works appropriately if the cyclist wants to reduce the training effort further.

**6.3.4 Impact of Data Sampling Rate.** We are also interested in the impact of the sampling rate. Fig. 21 (b) illustrates the performance of riding position classification when the sampling rate is decreased to 200, 400, 600, and 800 Hz compared with the original 1200 Hz. We observe high sampling rate will slightly improve the performance, and SMARCyPAD is not very sensitive to the change of sampling rate. Even if the sampling rate is decreased to 200 Hz, SMARCyPAD still reaches 89.18% accuracy, 88.98% precision, and 88.19% recall.

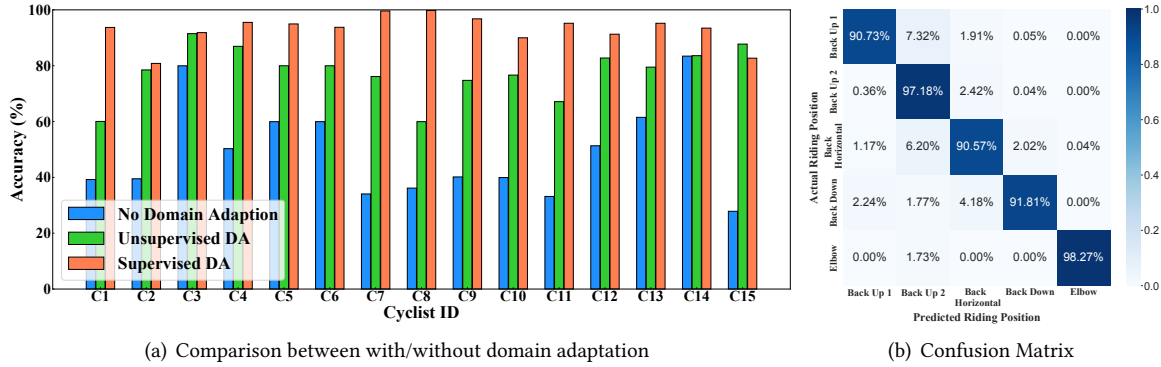


Fig. 20. Performance of riding position classification - cyclist-independent scenario.

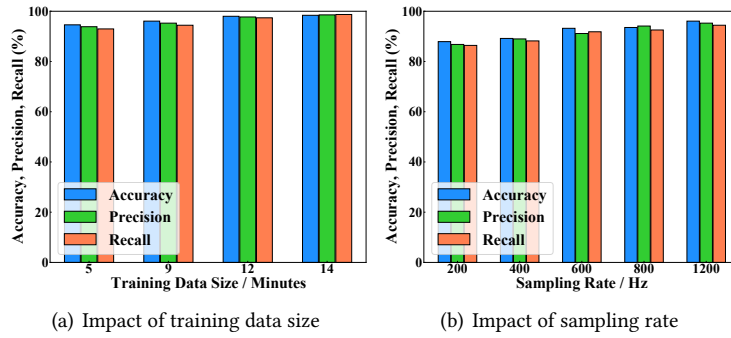


Fig. 21. Performance of riding position classification with different training data size &amp; sampling rate.

#### 6.4 Knee Joint Angle Regression

We use one participant's data to train the generic knee joint angle regressor, which has been shown to be sufficiently generalized and can be directly applied to all the other participants. Fig. 22 illustrates the average MAE and PCC of the knee joint angle for each cyclist. Specifically, we achieve an average MAE of 9.58 degrees and an average PCC of 87.14%, demonstrating SMARCyPAD can reconstruct the cyclist's knee joint angle with high performance. C3 reaches the lowest MAE of 6.78 degrees and the highest PCC of 94.22%, while C11 has the largest MAE & lowest PCC of 12.91 degrees & 77.13%, respectively. Fig. 23 illustrates an example of the reconstructed and ground truth knee joint angle series for a period of 25 seconds. We can observe that SMARCyPAD is able to capture the periodic pattern and the reconstructed knee joint angles are highly correlated and strictly synchronized with the groundtruth.

#### 6.5 Impact of Different Saddles

We further test the performance of SMARCyPAD on S2 and S3. The results for cadence estimation are presented in Fig. 24, in which we achieve an average MAE of 1.53 & 2.07% RE for S2, and 1.00 MAE & 1.49% RE for S3. Among all positions, “Elbow” performs best with 0.6 MAE and 0.82% RE on S2, while “Back Down” achieves only 0.58 MAE & 0.86% RE on S3. The results for riding position classification are shown in Fig. 25. Specifically,

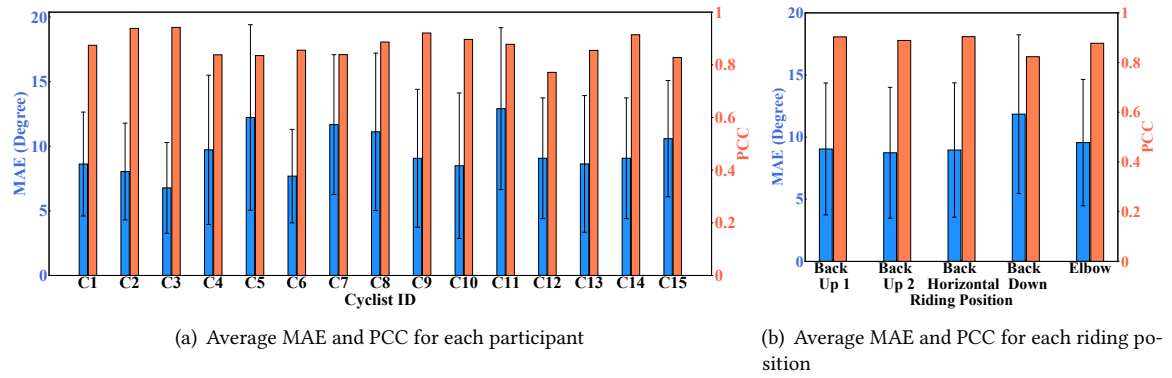


Fig. 22. Performance of knee angle regression.

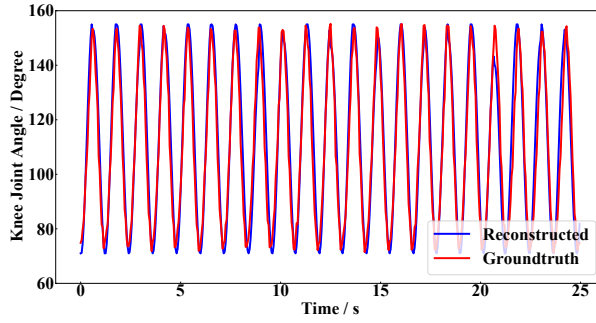
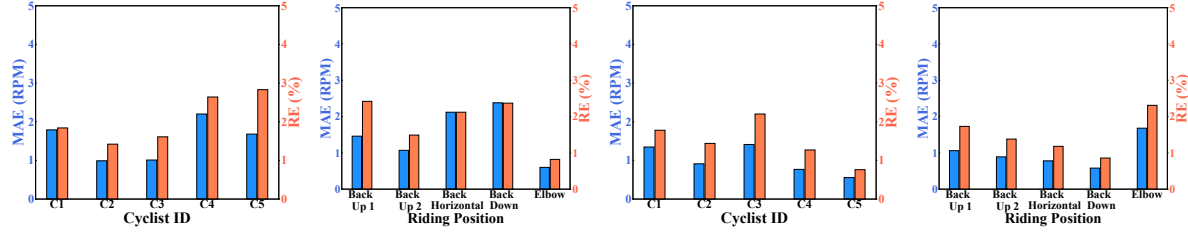


Fig. 23. Comparison between the reconstructed knee joint angle with the groundtruth.

under the cyclist-dependent scenario, the average accuracy, precision, and recall for S2 are 96.2%, 96.77%, and 95.94%, respectively, while 95.14%, 96.23%, and 95.72% for S3. As for the cyclist-independent scenario, the average accuracy for unsupervised domain adaptation is 73.78%/67.36% for S2/S3, while the accuracy for supervised domain adaptation is 91.41%/93.78%. Finally, as illustrated in Fig. 26, we achieve an average MAE/PCC of 9.75 degrees/87.01% on S2 and 8.77 degrees/85.87% on S3 for knee joint angle regression. In general, the performance of SMARCyPAD on S2 and S3 is comparable with S1, demonstrating its robustness with different saddles.

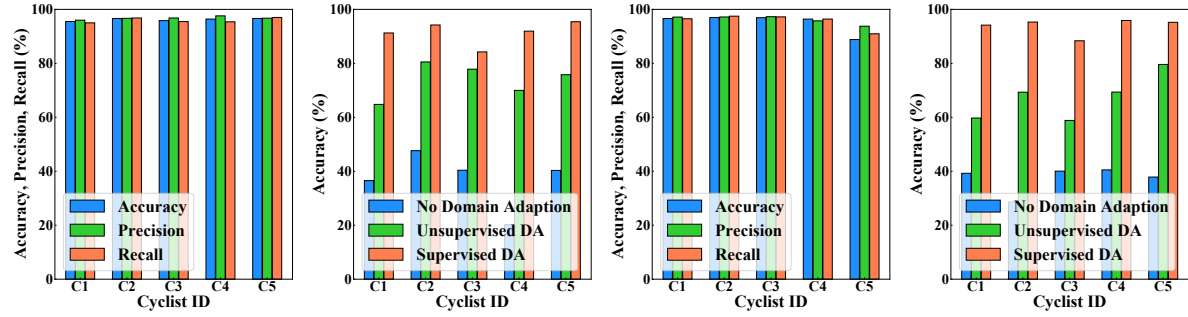
## 6.6 Temporal Stability

The accuracy of the deep learning model for riding position classification may be affected by various factors such as the sitting position of cyclists, their physical condition, and wear and tear caused by prolonged usage of the sensors. To test the temporal stability of SMARCyPAD, we ask two cyclists to collect another five sets of testing data (15 minutes each), which is separated from the training data by 1 day, 2 days, 1 week, 2 weeks, and over 1 month. Only 15 seconds of labeled data were utilized for supervised domain adaptation, which we believe can be easily achieved in practice. For example, the user can simply perform a brief warm-up by cycling with specific positions and following instructions for a few seconds before starting their fitness routine. The results are illustrated in Fig. 27: we found that SMARCyPAD maintains over 95% accuracy in a one-month period, and there is no significant performance change. These results prove the temporal stability of SMARCyPAD.



(a) Estimation error for each cyclist on S2 (b) Estimation error for each position on S2 (c) Estimation error for each cyclist on S3 (d) Estimation error for each position on S3

Fig. 24. Performance of cadence estimation on S2 & S3.



(a) Accuracy, precision, and recall on S2 - dependent scenario (b) Accuracy on S2 - independent scenario (c) Accuracy, precision, and recall on S3 - independent scenario (d) Accuracy on S3 - dependent scenario

Fig. 25. Performance of riding position classification on S2 & S3.

## 6.7 Computational Cost

Cadence, per-leg stability, and leg strength balance in SMARCYPAD only involve a few signal processing algorithms, such as filtering and peak detection, which require relatively light computational power, thus we only measure the computational cost of the riding position classification and knee joint angle reconstruction modules, which rely on machine learning. Specifically, we measure the inference time of distinguishing the five riding positions and reconstructing the knee joint angle on three different devices: a NVIDIA GTX 2080 GPU, a Macbook Pro 2019, and an NVIDIA Jetson Nano Board. The inference time for each second is only 0.042 ms on the 2080 GPU, 0.159 ms on the Macbook Pro, and 12.187 ms on the Jetson Nano Board, which is sufficient for real-time application.

## 6.8 User Study

We have asked all cyclists to complete a questionnaire on their experience with SMARCYPAD for user study. Each question has 5 different levels of ratings (e.g., Very willing, Willing, Maybe, Not willing, Very not willing). The results are illustrated in Fig. 28: we observe that 93.3% of the cyclists are willing to use SMARCYPAD, and only 1 cyclist chose “Maybe”. The specific reason is that the cyclist feels that the camera is more suitable for tracking riding postures, as it provides clearer visuals and is less susceptible to false predictions. Additionally, we found that all cyclists feel SMARCYPAD is comfortable and easy to use, and are satisfied with its performance. These high ratings demonstrate the willingness among cyclists to adopt SMARCYPAD for their cycling fitness tracking.

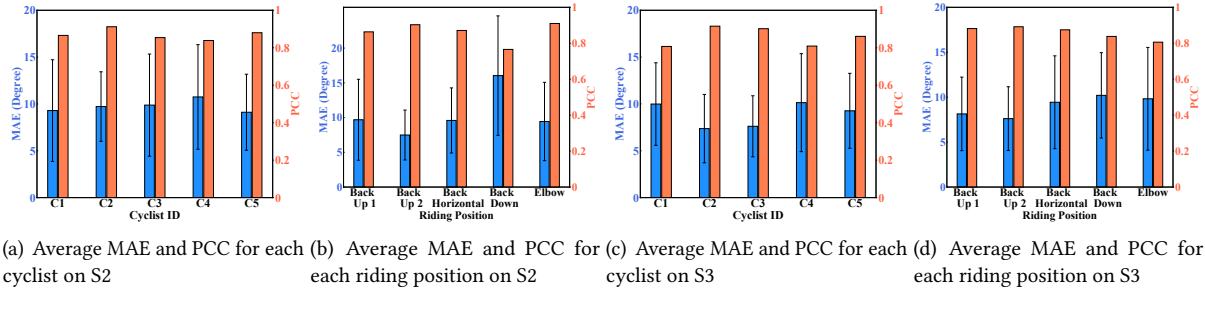


Fig. 26. Performance of knee joint angle regression on S2 &amp; S3.

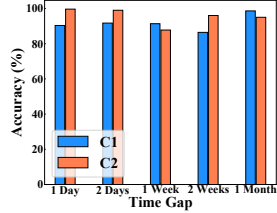


Fig. 27. Performance of riding position classification over time.

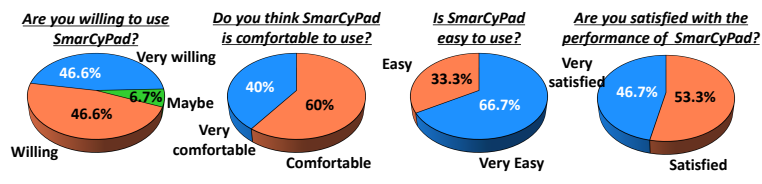


Fig. 28. Results of the user study questionnaire.

## 7 RELATED WORK

**Cycling Fitness Tracking.** Traditional cycling fitness tracking systems typically use cameras or IMU sensors (i.e., accelerometer, gyroscope, and magnetometer) to estimate the cyclists' riding positions & joint angles. Carranco *et al.* place a camera at the side of the cyclist, and it detects the coordinates of multiple body joints in 3D space leveraging computer-vision-based algorithms [25]. The posture of the cyclist and the joint angles are further derived by leveraging these coordinates. However, the proposed system can only monitor the joint angle of a single leg due to body occlusions and may raise serious privacy concerns. Alternatively, Cordillet *et al.* and Maio *et al.* achieve similar objectives through attaching multiple IMU sensors on the cyclist's body (e.g., torso, wrist, and knee) [26, 42]. Essential joint angles and body posture are further calculated using sensor fusion algorithms. Although IMU sensors are resilient to body occlusions and privacy preserving, deploying these on-body sensors can be cumbersome, and the cyclist's mobility and comfort could also be negatively affected. Moreover, IMU sensors are not suitable for long-term monitoring due to sensor drifting issues. Other than body postures and joint angles, there also exists cycling monitoring systems that focus on the basic body status of the cyclist (e.g., cycling speed, heart rate, and body temperature). Different types of sensors (e.g., speed sensors, heart rate sensors, temperature sensors) are attached to both the bicycles and the cyclists, with sensor measurements transmitted to the back-end server in real-time via Wireless Sensor Network (WRSN) [38, 45, 54] or WiFi [46]. Nevertheless, these studies mainly focus on reducing overhead on data transmission between the sensors and the back-end server. Furthermore, these studies can only track the primary body status of the cyclist (e.g., heart rate) while ignoring important cycling-specific information such as joint angles and seating positions. Unlike from these existing works, SMARCYPAD preserves the privacy of the cyclist, maintains the minimum obtrusiveness level to the cyclist, and monitors different types of cycling-specific information including cadence, seating position, and joint angles accurately.

**E-textile Sensing.** There has been active research on motion recognition and health monitoring leveraging e-textile sensors [34]. Existing studies have demonstrated that on-cloth fabric and fiber sensors can reconstruct joint angles of both the upper body [40] and the lower body [22, 28, 30, 31, 59]. In addition to joint angles, Kiaghadi *et al.* prove that on-sleeve fabrics can also monitor the user's sweating behavior [35]. Mattmann *et al.* attach thermoplastic elastomer strain sensor at the back of clothes to classify 27 upper body postures [44], Skach *et al.* place fabric sensors in trousers to distinguish 19 lower body postures [53], and Lorussi *et al.* embed fabric sensors into gloves for hand posture classification [41]. Additionally, Skach *et al.* build a smart seat cover using fabric sensors to detect the user's social behavior [52], while Ishac *et al.* develop a smart chair to monitor the user's seating posture [33]. Other than body motion monitoring, e-textile sensors have also been widely deployed for real-time health condition monitoring. Yan *et al.* use both fiber [61] and yarn [62] for healthcare monitoring. Pacelli *et al.* and Wang *et al.* embed smart fabric in clothes for breathing rate monitoring [49, 58], Lin *et al.* create a bedsheet composed of fabric sensor arrays for sleep monitoring [39], while Kiaghadi *et al.* achieve similar objective for sleep monitoring using a smart pyjama [36]. Different from these existing studies, we for the first time use pressure fabric for cycling monitoring, and the cyclist is not required to wear any on-body sensors.

## 8 CONCLUSION AND DISCUSSIONS

In this paper, we propose SMARCYPAD, a fabric-sensing-based smart seat pad for cycling fitness tracking. We design and manufacture SMARCYPAD from scratch leveraging off-the-shelf materials and develop a series of algorithms to accurately track five cycling-specific metrics of the cyclist. Extensive evaluations involving 15 participants demonstrate SMARCYPAD can estimate the cyclist's cadence with an average error of 1.13 RPM, quantify per-leg stability, detect cycling imbalance, distinguish riding position with an accuracy of 96.60%, and reconstruct knee joint angle with an average MAE of 9.58 degrees.

**Long-term Usage.** Our experiments are conducted over a ten-month period with over 94,500 riding cycles. SMARCYPAD preserves high performance throughout this period without any sensor replacement or maintenance, indicating its high durability. As an appropriate cycling time is only around 3 to 5 hours per week [10], we believe the current form is sufficiently good for long-term usage.

**Outdoor Cycling.** SMARCYPAD is mainly designed for immersive indoor cycling scenarios, yet we haven't tested its performance in outdoor scenarios or under unfavorable weather conditions such as rainy or windy environments. We believe SMARCYPAD can be readily extended to outdoor cycling, as the sensing signal pattern induced by cycling activities should remain consistent as long as the way of cycling (i.e., riding position) is unchanged, regardless of indoor or outdoor cycling. Meanwhile, as the contact between the user's hip and the bike saddle is relatively close, we believe environmental factors (e.g., rain and wind) will only have a subtle impact on the system's robustness since it's less likely for them to reach the sensing area. The evaluation of SMARCYPAD in outdoor scenarios is considered as our future work.

**Cycling-irrelevant Activities.** In this paper, we assume all unlabeled data for domain adaptation is related to cycling activities, while cyclists may perform cycling-irrelevant activities on the saddle (e.g., take a rest, or drink water), which may worsen the performance of domain adaptation. However, cycling-relevant activities (i.e., pedaling) usually exhibit a significantly higher frequency of body movements compared to these static activities. To the best of our knowledge, no activities performed while sitting on a bike saddle require frequent and periodic leg movements apart from cycling itself. Therefore, a high-pass filter can be used to effectively eliminate cycling-irrelevant noises. Additionally, the user could always perform a quick calibration (less than 1 minute) leveraging supervised domain adaptation if the classification results are not satisfied. We believe SMARCYPAD could work robustly and reliably if deployed in real-world settings.

**Waterproofness.** Some cyclists sweat a lot during the experiment, making the sensing prototype get wet. As the sensors and conductive threads are water-proof [17], we did not notice any effect on the system performance,

indicating the waterproofness of SMARCYPAD. In our current design, only the MCU and reference resistors are not water-proof, but they can be easily detached from the loop, as illustrated in Fig. 8 (i). We plan to evaluate the impact of both human wash and machine washing on the system performance, which is left as our future work.

**Large-scale Manufacturing.** The current manufacturing process of the sensing prototype takes many human efforts for cutting fabrics, tracing & sewing conductive threads, and insulating the sewed circuit. We want to seek the potential of using fabric sensing in the field of cycling fitness tracking. To enable large-scale manufacturing, we can automate and accelerate some of the steps in Section 4.3. For instance, the fabric pieces and conductive threads can be sliced & sewed automatically as they have fixed sizes, shapes, and diagrams. The electrical tapes can be replaced with other materials such as rubber silicon, which could be heated and glued along with the conductive threads for insulation. We believe the manufacturing process is highly repeatable and can potentially be automated by machines for large-scale manufacturing.

## ACKNOWLEDGMENTS

We would like to thank our anonymous reviewers for their insightful feedback. This work was supported in part by NSF grants CNS-2114161, ECCS-2132106, and CBET-2130643.

## REFERENCES

- [1] 2014. Body imbalance: Are you pedalling symmetrically? <https://www.cyclingweekly.com/fitness/training/power-symmetry-128109>.
- [2] 2018. Cycling 101: What Is Cadence & Why Is It Important? <https://www.flobikes.com/articles/6749522-cycling-101-what-is-cadence-why-is-it-important>.
- [3] 2021. HOW TO MEASURE SIT BONE WIDTH FOR BIKE SADDLE SIZE. <https://hincapie.com/ride-with-us/stories-from-the-saddle/how-to-measure-sit-bone-width-for-bike-saddle-size/#:~:text=Common%20bike%20saddle%20sizes%20range,discipline%2C%20and%20even%20personal%20preference..>
- [4] 2022. 26 BICYCLE INDUSTRY STATISTICS [2022]: MARKET SIZE, SHARE, GROWTH, AND TRENDS. <https://www.zippia.com/advice/bicycle-industry-statistics/>.
- [5] 2022. 43"x39" Faraday Fabric,EMF Protection Fabric,RFID Shielding Cloth Protection Conductive Fabric,Anti Radiation,Shielding Fabric Apply for Microwave, Card Bag Cloth, Electronic Products. [https://www.amazon.com/CALIDAKA-Protection-Shielding-Conductive-Electronic/dp/B08P43BQ6X/ref=sr\\_1\\_16?dchild=1&keywords=conductive%2Bfabric&qid=1630388452&sr=8-16&th=1](https://www.amazon.com/CALIDAKA-Protection-Shielding-Conductive-Electronic/dp/B08P43BQ6X/ref=sr_1_16?dchild=1&keywords=conductive%2Bfabric&qid=1630388452&sr=8-16&th=1).
- [6] 2022. Competitive e-cycling lets you be a champion from your apartment. <https://www.technologyreview.com/2022/01/10/1043281/e-cycling-swift-championships/#:~:text=Fitness%20platforms%20such%20as%20Peloton,doubled%20last%20year%2C%20it%20claims..>
- [7] 2022. Dritz 29500 Petite Press Portable Mini Iron,White. <https://www.amazon.com/Dritz-29500-Petite-Press-Portable/dp/B002N2GB3I>.
- [8] 2022. FLORA - Wearable electronic platform: Arduino-compatible - v3. <https://www.adafruit.com/product/659>.
- [9] 2022. Hammerhead Karoo 2. <https://www.hammerhead.io/products/hammerhead-karoo-2>.
- [10] 2022. How Many Hours Should Cyclists Ride for Fitness and Performance? <https://trainright.com/how-many-hours-should-cyclists-ride-fitness-performance-training/#:~:text=So%2C%20since%20cycling%20is%20typically,metabolic%20benefits%20of%20aerobic%20exercise..>
- [11] 2022. Iron ON Hemming Tape. <https://www.amazon.com/IKEA-4337014292-IRON-HEMMING-TAPE/dp/B005O9WU9Q>.
- [12] 2022. POWRLINK ZERO DUAL-SIDED POWER PEDALS. <https://www.wahofitness.com/devices/pedals/powrlink/powrlink-zero-dual-power-pedal-buy>.
- [13] 2022. Pressure-Sensitive Conductive Sheet (Velostat/Linqstat). <https://www.adafruit.com/product/1361>.
- [14] 2022. Sew Classics Microsuede Fabric. <https://www.joann.com/sew-classics-microsuede/xprd757799.html>.
- [15] 2022. SINGER | 4411 Heavy Duty Sewing Machine With Accessory Kit & Foot Pedal - 69 Stitch Applications - Simple & Great For Beginners. [https://www.amazon.com/SINGER-4411-Stitches-Stainless-Bedplate/dp/B003VWXZKG/ref=asc\\_df\\_B003VWXZKG/?tag=hvprod-20&linkCode=df0&hvadid=167136485511&hvpos=&hvnetw=g&hvrand=4837703140704576771&hvpcne=&hvptwo=&hvqmt=&hvdev=c&hvdvcndl=&hvlocint=&hvloctyp=9013451&hvtagid=pla-154925789290&th=1](https://www.amazon.com/SINGER-4411-Stitches-Stainless-Bedplate/dp/B003VWXZKG/ref=asc_df_B003VWXZKG/?tag=hvprod-20&linkCode=df0&hvadid=167136485511&hvpos=&hvnetw=g&hvrand=4837703140704576771&hvpcne=&hvptwo=&hvqmt=&hvdev=c&hvdvcndl=&hvlocint=&hvloctyp=9013451&hvtagid=pla-154925789290&th=1).
- [16] 2022. Stainless Thin Conductive Thread - 2 ply - 23 meter/76 ft. <https://www.adafruit.com/product/640>.
- [17] 2022. Washing Wearable Electronics. <https://learn.adafruit.com/washing-wearable-electronics>.
- [18] 2022. Swift. [https://us.swift.com/?utm\\_source=google&utm\\_medium=cpc&utm\\_campaign=swift\\_nam\\_us\\_cycling\\_search\\_brandcoreex\\_performance\\_eng\\_imprshare-21&gclid=CjwKCAjwpqCZBhAbEiwAa7pXeSde4cRsxp2pr9BifFY0yxVzKzqlY2yVDAAApwDaYrGTlpLXNA-TRoCjp4QAvD\\_BwE](https://us.swift.com/?utm_source=google&utm_medium=cpc&utm_campaign=swift_nam_us_cycling_search_brandcoreex_performance_eng_imprshare-21&gclid=CjwKCAjwpqCZBhAbEiwAa7pXeSde4cRsxp2pr9BifFY0yxVzKzqlY2yVDAAApwDaYrGTlpLXNA-TRoCjp4QAvD_BwE).

- [19] 2023. BLUEWIND Bike Seat, Bicycle Saddle Compatible with Peloton, Exercise or Road Bikes, 2in High Elastic Memory Foam Waterproof Dual Shock Absorbing Multi-Color Wide Cushion for Men & Women. <https://www.amazon.com/BLUEWIND-Comfortable-Bicycle-Memory-Waterproof/dp/B07QPG6C3V/>.
- [20] 2023. Wittkop Bike Seat I Bicycle Seat for Men and Women, Waterproof Bike Saddle with Innovative 5-Zone-Concept I Exercise Bike Seat for BMX, MTB & Road. <https://www.amazon.com/Wittkop-Bicycle-Saddle-Trekking-Bikes/dp/B0845PGYYZ/>.
- [21] Nathan Barry, David Burton, John Sheridan, Mark Thompson, and Nicholas AT Brown. 2015. Aerodynamic performance and riding posture in road cycling and triathlon. *Proceedings of the Institution of Mechanical Engineers, Part P: Journal of Sports Engineering and Technology* 229, 1 (2015), 28–38.
- [22] Jeroen HM Bergmann, Salzitsa Anastasova-Ivanova, Irina Spulber, Vivek Gulati, Pantelis Georgiou, and Alison McGregor. 2013. An attachable clothing sensor system for measuring knee joint angles. *IEEE Sensors Journal* 13, 10 (2013), 4090–4097.
- [23] Bert Blocken, Thijss van Druenen, Yasin Topalar, and Thomas Andrianne. 2018. Aerodynamic analysis of different cyclist hill descent positions. *Journal of Wind Engineering and Industrial Aerodynamics* 181 (2018), 27–45.
- [24] Z. Cao, G. Hidalgo Martinez, T. Simon, S. Wei, and Y. A. Sheikh. 2019. OpenPose: Realtime Multi-Person 2D Pose Estimation using Part Affinity Fields. *IEEE Transactions on Pattern Analysis and Machine Intelligence* (2019).
- [25] Jorge S Carranco, Francisco D Salgado, and O Alvarado Cando. 2016. Posture detection, classifier and correction system for cyclists applying KINECT V2 with neural nets and fuzzy logic. In *2016 IEEE Signal Processing in Medicine and Biology Symposium (SPMB)*. IEEE, 1–2.
- [26] Sébastien Cordillet, Nicolas Bideau, Benoit Bideau, and Guillaume Nicolas. 2019. Estimation of 3D knee joint angles during cycling using inertial sensors: Accuracy of a novel sensor-to-segment calibration procedure based on pedaling motion. *Sensors* 19, 11 (2019), 2474.
- [27] Jéssica da Silva Soares, Felipe P Carpes, Gislaine de Fátima Geraldo, Fabíola Bertú Medeiros, Marcos Roberto Kunzler, Álvaro Sosa Machado, Leopoldo Augusto Paolucci, and André Gustavo Pereira de Andrade. 2021. Functional data analysis reveals asymmetrical crank torque during cycling performed at different exercise intensities. *Journal of Biomechanics* 122 (2021), 110478.
- [28] Massimiliano Donno, Elia Palange, Fabio Di Nicola, Giovanni Bucci, and Fabrizio Ciancetta. 2008. A new flexible optical fiber goniometer for dynamic angular measurements: Application to human joint movement monitoring. *IEEE Transactions on Instrumentation and Measurement* 57, 8 (2008), 1614–1620.
- [29] Yaroslav Ganin and Victor Lempitsky. 2015. Unsupervised domain adaptation by backpropagation. In *International conference on machine learning*. PMLR, 1180–1189.
- [30] Mohsen Gholami, Andreas Ejupi, Ahmad Rezaei, Andrea Ferrone, and Carlo Menon. 2018. Estimation of knee joint angle using a fabric-based strain sensor and machine learning: A preliminary investigation. In *2018 7th IEEE International Conference on Biomedical Robotics and Biomechatronics (Biorob)*. IEEE, 589–594.
- [31] Peter T Gibbs and HHarry Asada. 2005. Wearable conductive fiber sensors for multi-axis human joint angle measurements. *Journal of neuroengineering and rehabilitation* 2, 1 (2005), 1–18.
- [32] Sergey Ioffe and Christian Szegedy. 2015. Batch normalization: Accelerating deep network training by reducing internal covariate shift. In *International conference on machine learning*. PMLR, 448–456.
- [33] Karlos Ishac and Kenji Suzuki. 2018. Lifechair: A conductive fabric sensor-based smart cushion for actively shaping sitting posture. *Sensors* 18, 7 (2018), 2261.
- [34] GM Nazmul Islam, Azam Ali, and Stewart Collie. 2020. Textile sensors for wearable applications: A comprehensive review. *Cellulose* 27 (2020), 6103–6131.
- [35] Ali Kiaghadi, Morgan Baima, Jeremy Gummesson, Trisha Andrew, and Deepak Ganesan. 2018. Fabric as a sensor: Towards unobtrusive sensing of human behavior with triboelectric textiles. In *Proceedings of the 16th ACM Conference on Embedded Networked Sensor Systems*. 199–210.
- [36] Ali Kiaghadi, Seyedeh Zohreh Homayounfar, Jeremy Gummesson, Trisha Andrew, and Deepak Ganesan. 2019. Phyjama: physiological sensing via fiber-enhanced pyjamas. *Proceedings of the ACM on Interactive, Mobile, Wearable and Ubiquitous Technologies* 3, 3 (2019), 1–29.
- [37] CR Kyle and MD Weaver. 2004. Aerodynamics of human-powered vehicles. *Proceedings of the Institution of Mechanical Engineers, Part A: Journal of Power and Energy* 218, 3 (2004), 141–154.
- [38] NM Abdul Latiff, MA Ruslee, SK Syed Yusof, MR Abdul Rahim, H Sayuti, K Mohamad Yusof, and MA Baharudin. 2017. A training monitoring system for cyclist based on wireless sensor networks. *Indonesian Journal of Electrical Engineering and Computer Science* 6, 1 (2017), 80–87.
- [39] Zhiming Lin, Jun Yang, Xiaoshi Li, Yufen Wu, Wei Wei, Jun Liu, Jun Chen, and Jin Yang. 2018. Large-scale and washable smart textiles based on triboelectric nanogenerator arrays for self-powered sleeping monitoring. *Advanced Functional Materials* 28, 1 (2018), 1704112.
- [40] Ruibo Liu, Qijia Shao, Siqi Wang, Christina Ru, Devin Balkcom, and Xia Zhou. 2019. Reconstructing human joint motion with computational fabrics. *Proceedings of the ACM on Interactive, Mobile, Wearable and Ubiquitous Technologies* 3, 1 (2019), 1–26.
- [41] Federico Lorussi, Enzo Pasquale Scilingo, Mario Tesconi, Alessandro Tognetti, and Danilo De Rossi. 2005. Strain sensing fabric for hand posture and gesture monitoring. *IEEE transactions on information technology in biomedicine* 9, 3 (2005), 372–381.

- [42] António F Maio and José A Afonso. 2015. Wireless cycling posture monitoring based on smartphones and bluetooth low energy. (2015).
- [43] Alexander James Marsden, DG Papageorgiou, Cristina Valles, A Liscio, V Palermo, MA Bissett, RJ Young, and IA Kinloch. 2018. Electrical percolation in graphene–polymer composites. *2D Materials* 5, 3 (2018), 032003.
- [44] Corinne Mattmann, Oliver Amft, Holger Harms, Gerhard Troster, and Frank Clemens. 2007. Recognizing upper body postures using textile strain sensors. In *2007 11th IEEE international symposium on wearable computers*. IEEE, 29–36.
- [45] Nurul Muâ, Mohd Musa Mohamad, Sharifah Kamilah Syed Yusof, Mohd Rozaini Abd Rahim, Hamdan Sayuti, Nik Noordini Nik Abdul Malik, et al. 2013. Training monitoring system for cyclist based on android application development. *Jurnal Teknologi* 64, 3 (2013).
- [46] Wan Norsyafizan W Muhamad, Sayyidul Ainulfadhil bin Razali, Norfishah Ab Wahab, Meor Mohd Azreen, Suzi Seroja Sarnin, and Nani Fadzlin Naim. 2020. Smart Bike Monitoring System for Cyclist via Internet of Things (IoT. In *2020 IEEE 5th International Symposium on Telecommunication Technologies (ISTT)*. IEEE, 168–173.
- [47] Rita Paradiso, Laura Caldani, and Maria Pacelli. 2014. Knitted electronic textiles. In *Wearable Sensors*. Elsevier, 153–174.
- [48] Fabian Pedregosa, Gaël Varoquaux, Alexandre Gramfort, Vincent Michel, Bertrand Thirion, Olivier Grisel, Mathieu Blondel, Peter Prettenhofer, Ron Weiss, Vincent Dubourg, et al. 2011. Scikit-learn: Machine learning in Python. *the Journal of machine Learning research* 12 (2011), 2825–2830.
- [49] Enzo Pasquale Scilingo, Angelo Gemignani, Rita Paradiso, Nicola Taccini, Brunello Ghelarducci, and Danilo De Rossi. 2005. Performance evaluation of sensing fabrics for monitoring physiological and biomechanical variables. *IEEE Transactions on information technology in biomedicine* 9, 3 (2005), 345–352.
- [50] Fred Shaffer and Jay P Ginsberg. 2017. An overview of heart rate variability metrics and norms. *Frontiers in public health* (2017), 258.
- [51] Marc R Silberman. 2013. Bicycling injuries. *Current sports medicine reports* 12, 5 (2013), 337–345.
- [52] Sophie Skach, Patrick GT Healey, and Rebecca Stewart. 2017. Talking Through Your Arse: Sensing Conversation with Seat Covers.. In *CogSci*.
- [53] Sophie Skach, Rebecca Stewart, and Patrick GT Healey. 2018. Smart arse: posture classification with textile sensors in trousers. In *Proceedings of the 20th ACM International Conference on Multimodal Interaction*. 116–124.
- [54] Sukhairi Sudin, Ali Yeon Md Shakaff, Fezri Aziz, Fathinul Syahir Ahmad Saad, Ammar Zakaria, and Ahmad Faizal Salleh. 2016. Track cyclist performance monitoring system using wireless sensor network. In *Regional Conference on Science, Technology and Social Sciences (RCSTSS 2014)*. Springer, 123–131.
- [55] Amina Tihak and Dušanka Bošković. 2019. Experimental evaluation of challenges in designing a resistive pressure sensors. In *IEEE EUROCON 2019-18th International Conference on Smart Technologies*. IEEE, 1–6.
- [56] Eric Tzeng, Judy Hoffman, Trevor Darrell, and Kate Saenko. 2015. Simultaneous deep transfer across domains and tasks. In *Proceedings of the IEEE international conference on computer vision*. 4068–4076.
- [57] Pauli Virtanen, Ralf Gommers, Travis E Oliphant, Matt Haberland, Tyler Reddy, David Cournapeau, Evgeni Burovski, Pearu Peterson, Warren Weckesser, Jonathan Bright, et al. 2020. SciPy 1.0: fundamental algorithms for scientific computing in Python. *Nature methods* 17, 3 (2020), 261–272.
- [58] Lie Wang, Liyuan Wang, Ye Zhang, Jian Pan, Shangyu Li, Xuermei Sun, Bo Zhang, and Huisheng Peng. 2018. Weaving sensing fibers into electrochemical fabric for real-time health monitoring. *Advanced Functional Materials* 28, 42 (2018), 1804456.
- [59] Amanda Watson, Minglong Sun, Samhita Pendyal, and Gang Zhou. 2020. TracKnee: Knee angle measurement using stretchable conductive fabric sensors. *Smart Health* 15 (2020), 100092.
- [60] Sanghyun Woo, Jongchan Park, Joon-Young Lee, and In So Kweon. 2018. Cbam: Convolutional block attention module. In *Proceedings of the European conference on computer vision (ECCV)*. 3–19.
- [61] Tao Yan, Zhe Wang, and Zhi-Juan Pan. 2018. A highly sensitive strain sensor based on a carbonized polyacrylonitrile nanofiber woven fabric. *Journal of Materials Science* 53, 16 (2018), 11917–11931.
- [62] Tao Yan, Zhe Wang, Yi-Qi Wang, and Zhi-Juan Pan. 2018. Carbon/graphene composite nanofiber yarns for highly sensitive strain sensors. *Materials & Design* 143 (2018), 214–223.